Reciprocal regulation of p21 and Chk1 controls the Cyclin D1-RB pathway to mediate senescence onset after G2 arrest

Gerald Lossaint[1,2]*, Anđela Horvat[3]*, Véronique Gire[4], Katarina Bacevic[1], Karim Mrouj[1,5], Fabienne Charrier-Savournin[4,6], Virginie Georget [4,7], Daniel Fisher[1], and Vjekoslav Dulic[1]#

1. IGMM, Univ. Montpellier, CNRS, Montpellier, France

2. Present address: Institut du cancer de Montpellier, Montpellier, France

3. Ruđer Bošković Institute, 10000 Zagreb, Croatia

4. CRBM, Univ. Montpellier, CNRS, Montpellier, France

5. Present address: Stanford University School of Medicine, Stanford, USA

6. Present address: PerkinElmer, Inc., Parc Marcel Boiteux, BP 84175 30200 Codolet, France

7. Montpellier Ressources Imagerie, BioCampus, University of Montpellier, CNRS, INSERM, Montpellier, France

* These authors contributed equally to this work

#Contact information: Vjekoslav Dulic, Tel.: +33 4 34 35 96 77

E-mail: vjekoslav.dulic@igmm.cnrs.fr

e-mail addresses:

gerald.lossaint@icm.unicancer.fr

Andjela.Horvat@irb.hr

Veronique.Gire@crbm.cnrs.fr

katarinabacevic@gmail.com

karim.mrouj@stanford.edu

Fabienne.CharrierSavournin@perkinelmer.com

virginie.georget@mri.cnrs.fr

daniel.fisher@igmm.cnrs.fr

Keywords: senescence, DNA damage, G2 arrest, Cyclin D, RB, p21, Chk1, CDK6

Summary

Senescence is an irreversible proliferation withdrawal that can be initiated after DNA damage-induced cell cycle arrest in G2 phase to prevent genomic instability. Senescence onset in G2 requires p53 and RB family tumour suppressors, but how they are regulated to convert a temporary cell cycle arrest into a permanent one remains unknown. Here, we show that a previously unrecognised balance between the CDK inhibitor p21 and Chk1 controls D-type cyclin-CDK activity during G2 arrest. In non-transformed cells, p21 activates RB in G2 by inhibiting Cyclin D1-CDK2/CDK4. The resulting G2 exit, which precedes appearance of senescence markers, is associated with a mitotic bypass, Chk1 downregulation and DNA damage foci reduction. In p53/RB-proficient cancer cells, compromised G2 exit correlates with sustained Chk1 activity, delayed p21 induction, untimely Cyclin E1 re-expression and genome reduplication. Conversely, Chk1 depletion promotes senescence by inducing p21 binding to Cyclin D1 and Cyclin E1-CDK complexes and down-regulating CDK6, whereas Chk2 knockdown enables RB

phosphorylation and delays G2 exit. In conclusion, p21 and Chk2 oppose Chk1 to maintain RB activity, thus promoting DNA damage-induced senescence onset in G2.

Summary statement

Senescence onset after G2 arrest, which requires Chk1 downregulation and inhibition of CycD1-CDK complexes by p21 leading to RB activation, is compromised in cancer cells due to delayed p21 induction and sustained Chk1 activity.

Introduction

Senescence is an essentially permanent proliferation withdrawal that can be induced by diverse stimuli such as dysfunctional telomeres, DNA damage, excessive mitogenic signalling or oncogene activation (Di Micco et al., 2021). Senescent cells are characterized by hypertrophy, intense metabolic activity, increased β-galactosidase (SA-β-gal) activity, chromatin remodelling and enhanced secretion of proinflammatory molecules, known as the senescence-associated secretory phenotype (SASP; Sharpless and Sherr, 2015; Roger et al., 2021) In addition to preventing neoplastic transformation, senescence plays an important role in a number of physiological and pathological processes contributing to age-related disorders and cancer (Di Micco et al., 2021; He and Sharpless, 2017).

Irreversible cell cycle arrest precedes the appearance of the routinely used markers of senescence (SA-β-gal), and it requires functional p53 and retinoblastoma protein (RB)-family tumour suppressors (Sharpless and Sherr, 2015). In replicative senescence, G1 arrest is mediated by the p53-induced CDK inhibitor $p21^{Waf1/Cip1}$ (p21), which inhibits G1 cyclin (CycD1 and CycE1)-bound CDKs, thereby blocking inactivating phosphorylation of RB family pocket proteins and preventing DNA replication (Dulic et al., 2000; Stein et al., 1999). This stable G1 arrest does not require the CDK4/CDK6-specific inhibitor $p16^{INK4A}$ (p16), which accumulates only in late stages of senescence and ensures its irreversibility by preventing formation of CycD1-CDK4/CDK6 complexes (Alcorta et al., 1996; He and Sharpless, 2017; Ito et al., 2018; Sharpless and Sherr, 2015; Stein et al., 1999).

Senescence can be also triggered in G2 phase of the cell cycle (Gire and Dulic, 2015; Shaltiel et al., 2015). DNA damage-induced G2 arrest is initiated by ATM/ATR–mediated phosphorylation of checkpoint kinases Chk1 and Chk2, which, by inhibiting CDC25 phosphatases, block activation of the mitosis inducer CDK1 (Chen and Poon, 2008). Converting a temporary G2 arrest into a permanent cell cycle arrest, termed G2 exit, which precedes appearance of full senescent phenotype markers, requires p21. In addition to inhibiting CycA-CDK1/2 (Bacevic et al., 2017a; Baus et al., 2003; Lossaint et al., 2011), thereby preventing CycB1-CDK1 activation (Lemmens and Lindqvist, 2019), p21 sequesters inactive CycB1-CDK1 in the nucleus (Charrier-Savournin et al., 2004; Krenning et al., 2014). This leads to downregulation of CycB1 and other mitotic regulators (Charrier-Savournin et al., 2004; Lossaint et al., 2011) *via* APC/C^{Cdh1}-mediated

degradation (Shaltiel et al., 2015). The G2 exit, which probably equates with senescence onset, is preceded by mitotic bypass, giving rise to stably arrested tetraploid G1 cells (Gire and Dulic, 2015; Johmura et al., 2014; Krenning et al., 2014). Additionally, p21 inhibits phosphorylation of RB family pocket proteins (Baus et al., 2003; Johmura et al., 2014) that leads to repression of E2F-dependent G2/M regulators (Jackson et al., 2005; Johmura et al., 2014; Sadasivam and DeCaprio, 2013). However, the identity of the RB kinase(s) that are targeted by p21 to trigger G2 exit has not been established. While CycD1-associated CDK4 and CDK6 promote G1/S progression by phosphorylating and inactivating RB (Chung et al., 2019; Topacio et al., 2019), the role of the CycD1-RB module after the restriction point remains under-studied. Unlike CycE1, CycD1 is also expressed in late cell cycle phases (Chassot et al., 2008; Gookin et al., 2017; Hitomi and Stacey, 1999; Matsushime et al., 1994; Yang et al., 2006). It is therefore possible that, like at G1/S transition (Lundberg and Weinberg, 1998), CycD1-CDKs "prime" RB enabling further phosphorylation by CDK2 and/or CDK1. This is consistent with a CycD1 role as a sensor/effector of anti-proliferative cues whose G2 levels control the proliferation-quiescence decision (Min et al., 2020; Yang et al., 2017b). However, whether the CycD1-RB module senses DNA damage in G2 has not been investigated.

Permanent G2 exit was proposed to serve as a safeguard mechanism preventing adaptation to the G2/M checkpoint (Baus et al., 2003), *i.e.* passage into mitosis of cells with damaged DNA, which can occur in cells lacking sufficient Chk1 activity (Feringa et al., 2018; Shaltiel et al., 2015). G2/M checkpoint adaptation also occurs in the absence of p53 or p21, and subsequent cytokinesis failure can lead to accumulation of

polyploid nuclei or cell death (Bunz et al., 1998; Johmura et al., 2014). Alternatively, in p53-deficient cells experiencing persistent telomere dysfunction, prolonged G2 arrest entails mitotic bypass and genome reduplication (Davoli et al., 2010), generating genomic instability (Davoli and de Lange, 2012), and coincides with sustained Chk1 and Chk2 activity. These results imply that, like p21, Chk1/Chk2 kinases stabilise the G2 arrest following continuous DNA damage, and suggest a certain redundancy between the two pathways. They also show that stable G2 arrest is not equivalent with, and does not necessarily lead to G2 exit. Paradoxically, although recent work implicated ATR/Chk1 in senescence onset in G2 (Feringa et al., 2018; Johmura et al., 2016), DNA damage-induced senescence or terminal differentiation are all invariably associated with Chk1 downregulation (Gabai et al., 2008; Gottifredi et al., 2001; Gire, 2004; Lossaint et al., 2011; Park et al., 2015; Ullah et al., 2011). It is currently unclear whether Chk1 signalling shutdown is required for the permanent cell cycle arrest or is merely a consequence.

In this study, we investigated the kinase network that controls the transition between DNA damage-induced G2 arrest and permanent G2 exit preceding senescence. We found that in non-transformed cells the G2 exit is driven by p21-dependent inhibition of CycD1-CDK complexes, which blocks RB phosphorylation and coincides with Chk1 but not Chk2 downregulation. We further show that sustained Chk1 activation in cancer cells is associated with impaired G2 exit and endoreplication, whereas its acute depletion strongly accelerated permanent cell cycle exit *via* p21-mediated inhibition of RB kinases. Our results suggest that, due to opposing regulation

of RB phosphorylation, Chk1 inhibits, whereas p21 and Chk2 promote, the onset of senescence in G2. Finally, we uncover CDK6 downregulation as an important component of the CycD1-RB pathway control during DNA damage-induced cell cycle exit in cancer cells.

Results

CycD1 and CycE1 accumulate upon DNA damage-induced G2 arrest prior to cell cycle exit and senescence

RB and p21 play key roles both in senescence (Chicas et al., 2010; Herbig et al., 2004; Yosef et al., 2017; Sturmlechner et al., 2021) and in DNA damage-induced permanent cell cycle arrest in G2 (Baus et al., 2003; Johmura et al., 2014). As such, the p21-mediated inhibition of RB kinases might be a key event triggering the switch between temporary and permanent G2 arrest (hereafter G2 exit) that precedes senescence onset. Since in human diploid fibroblasts (HDF) CycD1 is expressed after the G1/S transition (Chassot et al., 2008; Yang et al., 2017b) along with increased CycD1-specific RB phosphorylation (P^{S780}; Geng et al., 2001; Kitagawa et al., 1996), and its levels specifically decrease upon serum depletion coinciding with apparition of hypo-phosphorylated RB (Fig. 1A), we surmised that the CycD1-RB module could serve as a sensor for anti-proliferative cues even in late cell cycle phases. We therefore investigated whether p21 inhibits RB phosphorylation and promotes DNA damage-induced senescence onset in G2 by targeting CycD1-CDK complexes.

To test this hypothesis, we exposed HDF to genotoxic drugs, previously shown to induce G2 exit: ICRF-193, a DNA topoisomerase II inhibitor, which generates double strand DNA breaks in G2 phase, or bleomycin, a radiomimetic drug that causes G1 or G2 arrest (Fig. S1A, Baus et al., 2003). After 48h, both drugs inhibited RB phosphorylation and reduced RB levels (Broude et al., 2007), down-regulated CycA and Ki67, and induced accumulation of p21 and hypo-phosphorylated p130, a DREAM complex member (Sadasivam and DeCaprio, 2013) Fig. 1B-D). These hallmarks of permanent cell cycle arrest, observed also upon irradiation and in replicative senescence (Fig. 1B, E), invariably preceded later induction of senescent markers such as an increase of nuclear size (Fig. 1F), upregulation of CDK4/6 inhibitor p16 and acquisition of SA-β-gal staining (Fig. 1E,F and Fig. S1B,C). This shows that cell cycle exit precedes and is not equivalent to senescence. In addition, both G1 and G2 cell cycle arrests led to accumulation of CycE1 and CycD1, which is also observed in senescent cells (Fig. 1B, E; Dulic et al., 1993). Whereas CycE1 accumulated in p21-bound complexes only after CycA degradation as a result of mitotic bypass (Fig. 1B,E and Fig. S1D), single cell immunofluorescence showed that CycD1 increased already in G2-arrested cells, as documented by co-expression with CycA and CycB1 (Fig. 1G,H and Figs. S1E,F). Thus, cyclin D1 stabilization after G2 arrest might be an early marker of G2 exit.

p21 targets CycD1 to inhibit RB phosphorylation and promote senescence onset after G2 arrest

Next, we asked whether p21 targets CycD1-CDK complexes in G2-arrested cells, thereby inhibiting RB phosphorylation. Indeed, as shown by immunofluorescence (Fig. 2A-D) and immunoblots of p21 and CycD1 immunoprecipitates (Fig. 2E,F), G2 arrest correlated with increasing co-expression and binding of both CycD1 and CycA with p21 (Fig. 2E, F). Interestingly, in addition to CycD1-CDK4, G2-arrested cells also accumulated CycD1-CDK2 complexes (Fig. 2F), which also accumulate in senescent fibroblasts (Dulic et al., 1993; Stein et al., 1999). These data show that p21 simultaneously binds CycA-CDK1/2 that drives mitosis, and CycD1-CDK2/4/6 complexes, that phosphorylate RB. Consequently, preventing p21 induction might stimulate CycD1-dependent RB phosphorylation after G2 arrest. Indeed, CycD1-specific RB phosphorylation (P^{S780}) was promoted by p21 knock-down (KD) in HDF or human mammary epithelial cells (HMEC; Fig 2G) or expression of HPV16-E6 oncoprotein (Fig. S2A), which degrades p53 and prevents p21 induction (Baus et al., 2003) thereby compromising the cell cycle exit (Figs. S2B-C). Moreover, p21 KD prevented DNA damage-induced upregulation of Cyc D1 (Fig 2G) and, consequently, accumulation of CycD1-CDK2/4/6 complexes in G2-arrested cells (Fig. 2H). While these results are in agreement with the proposed role of p21 in stabilizing CycD1 (Chen et al., 2013) and confirm p21-dependent inhibition of CycD1-specific RB phosphorylation, they might also link accumulation of p21-CycD1-CDK complexes to G2 exit and senescence onset.

To further corroborate the role of CycD1-CDK complexes in phosphorylating RB beyond the G1/S transition, we knocked down CycD1 in proliferating HDF. Indeed, in cycling cells CycD1 KD strongly reduced expression and phosphorylation of both RB and p130 despite unchanged CycE1 and CycA levels (Fig. 2I), suggesting that Cdk2 associated with these cyclins cannot compensate for RB phosphorylation by CycD1-CDK complexes. Indeed, CycE1 KD failed to reduce CycD1-specific RB phosphorylation on Ser780 and little affected overall RB and p130 phosphorylations in cycling cells (Fig. 2I). Moreover, CycD1 KD also reduced p21 induction by ICRF-193 (Fig. 2I, IC-48h), which is consistent with CycD1-CDK complexes being major p21 targets after DNA damage.

Finally, to validate the key role of RB in DNA damage-induced G2 arrest/exit transition, we conditionally expressed SV40 large T antigen mutant (T_{121}), which specifically inactivates RB orthologs after addition of doxycycline (Conklin et al., 2012). Upon prolonged DNA damage treatment, RB family inactivation impaired both the cell cycle arrest and senescence onset despite high p21 levels, as shown by strong Ki-67 and CycA expression (Fig. 2J and Figs. S2D,E). Collectively, these results suggest that p21 initiates G2 cell cycle exit and subsequent senescence onset by binding to and inhibiting CycD1-CDK complexes, thereby blocking RB phosphorylation after G2 arrest (Fig. S2F).

Chk1 activity drives G2 arrest but its p53-dependent downregulation associates with G2 exit

Next, we asked whether p21 is sufficient to ensure stable G2 arrest preceding G2 exit or if it acts in synergy with Chk1/Chk2 checkpoint kinases. The robustness of the G2/M checkpoint depends on the level of DNA damage above a certain threshold (Lobrich and Jeggo, 2007). Therefore, the maintenance of G2 arrest and its conversion to a permanent G2 exit might depend on the strength of DNA damage signalling, with higher levels translating into increased Chk1/Chk2 activity and/or p21 induction. To test this hypothesis, HDF were synchronized in early S-phase (favouring G2 arrest) by release from contact inhibition and exposed to two different γ-ray doses (5 and 10 Gy) or bleomycin (24h; Fig. S3A). Both doses upregulated p21 and induced cell cycle exit, as documented by accumulation of hypo-phosphorylated p130, inhibition of RB phosphorylation, downregulation of RB and CycA, and stabilisation of G1 cyclins (Fig. 3A). However, whereas after 10 Gy cells arrested predominantly in the G2 phase, at 5 Gy most cells entered mitosis and arrested in G1 (Fig. 3B, and Fig. S3A). Accordingly, robust G2 arrest correlated with initially stronger Chk1 phosphorylation (Fig. 3A, 10 Gy). In contrast, despite stronger p53 phosphorylation after 10 Gy, p21 induction and Chk2 phosphorylation were comparable between the two γ-ray doses (Fig. 3A). This suggests that the intensity and persistence of Chk1 activation, rather than p21 levels, determines whether cells will arrest and exit the cell cycle in G2, or progress into mitosis and exit in G1. If this is true, then stronger Chk1 activation should confer more robust G2 arrest even if cells cannot induce p21. Indeed, at 10 Gy most p53-deficient E6-expressing

cells exhibiting elevated Chk1 phosphorylation arrested in G2, whereas at 5 Gy they progressed into the next cell cycle as shown by FACS analysis (Fig. 3C,D and Fig. S3B). These results were further corroborated by time-lapse studies showing that stronger and sustained Chk1 activation by bleomycin correlated with a robust G2 arrest, whereas HDF-E6 treated with ICRF-193 exhibiting more transient Chk1 phosphorylation, entered mitosis despite Chk2 activation (Fig. 3E,F and Fig. S3C). Similar conclusions regarding the role of Chk1 in stabilizing G2 arrest were obtained with another cellular model (Johmura et al., 2016). However, in agreement with our previous observations (Baus et al., 2003), both G1- and G2-arrested HDF-E6 cells failed to exit the cell cycle, as documented by persistent RB hyper-phosphorylation and Ki67 expression (Fig. 3D, Fig. S2A,B).

Surprisingly, given its key role in stabilizing G2 arrest, Chk1 phosphorylation and protein levels decreased before the onset of cell cycle exit (24h), contrasting with continuous Chk2 and p53 phosphorylations (Fig. 3A, lower panel). This transient nature of Chk1 phosphorylation was not specific to irradiation since it was also observed in cells exposed to bleomycin or ICRF-193 (Fig. S3C,D). By contrast, both Chk1 phosphorylation and protein levels were maintained in HDF-E6 arrested in G2 by radiation or bleomycin (Fig. 3D,F). Thus, sustained Chk1 phosphorylation was associated with impaired cell cycle exit. Conversely, Chk1 was strongly downregulated both in DNA damage-induced and replicative senescence (Fig. S3E,F). Taken together, these results highlight a correlation between the onset of G2 exit and suppression of Chk1,

but not Chk2, signalling by the p53/p21 pathway suggesting their differential roles in G2 arrest-to-G2 exit conversion.

G2 exit associates with γH2AX downregulation and reduction of DNA damage foci

We wondered if Chk1 downregulation might be a part of general DNA damage signalling switch-off associated with the onset of G2 exit. To explore this possibility, we analysed by immunofluorescence the γH2AX signal intensity and the number of DNA damage-induced foci at different times after exposure to ICRF-193, in both wild-type and E6-expressing HDF. As predicted, G2 exit (48-72h) correlated with a marked reduction of both number of γH2AX/53BP1 foci and γH2AX signal, which were strongly attenuated by E6-expression (Fig. 4A-D). It is unlikely that the observed downregulation of the DNA damage response signalling is due to DNA damage repair (Chowdhury et al., 2005) or checkpoint recovery (Macurek et al., 2010) since the experimental conditions induced massive DNA damage, causing senescence. Moreover, reduction of γH2AX/53BP1 foci correlated with an increase in foci size (Fig. 4A,B), which might reflect their clustering associated with delayed repair. These large foci resemble 53BP1 nuclear bodies that form in the G1 phase after unrepaired DNA damage or unresolved replication stress in the preceding cycle (Lukas et al., 2011). Significantly, in addition to the absence of Chk1 phosphorylation (Fig. S3E,F), most senescent cells also exhibited low γH2AX signal and reduced number of larger DNA damage foci (Fig. 4E). Based on our results, we suggest the G2 exit and implementation of senescence onset involves downregulation of Chk1 and ATM/ATR signalling *via* the p53/RB pathway (Fig. 4F).

Sustained Chk1 activity in G2-arrested U2OS cells coincides with altered mitotic bypass and delayed G2 exit

If G2 exit requires Chk1 downregulation, then one might expect that prolonged Chk1 activity due to sustained DNA damage, previously observed in p53/RB-proficient cancer cell lines (Lossaint et al., 2011) or p53-deficient cells (Davoli et al., 2010), would be incompatible with its onset. To address this hypothesis, we studied U2OS osteosarcoma cells that, when exposed to genotoxic agents, arrest predominantly in G2 due to a deficient ATM signalling, retarded p21 induction and persistent Chk1 activation (Fig. S4A,B; Kleiblova et al., 2013; Lossaint et al., 2011). Similarly, γ-irradiation (IR) led to delayed p21 induction and sustained dose-dependent Chk1 phosphorylation, whose intensity correlated well with robustness of G2 arrest as documented by FACS analysis and prolonged presence of CycB1 in cells exposed to 10 Gy irradiation (Fig. 5A,B, upper panel and Fig. S4A,B).

Consistent with our hypothesis, cell cycle exit was strongly impaired in G2-arrested U2OS cells, as documented by persistent RB hyperphosphorylation and CycA expression in both irradiated and cells exposed to genotoxic agents (Fig. 5B-lower panel and Fig. S4C-E). In addition, immunofluorescence results showed that in bleomycin- and ICRF-193-treated cells re-accumulation of CycE1 occurred before CycA downregulation, revealing the alteration of mitotic bypass associated with DNA re-replication (Fig. 5B,C and Fig. S5A-D). However, extended G2 arrest entailed strong upregulation of D-type cyclins, which correlated with p21 induction and its increased co-expression with CycE1 (Fig. 5B-F; Figs. S4B,C and S5E-G). Concomitant decrease of CycA-positive cells and increase of hypo-phosphorylated RB and p130 (Fig 5B,C, Figs. S4C and S5A,E) indicated the onset of G2 arrest/G2 exit conversion that coincided with nuclear size augmentation (Fig. 5C,E,G). Indeed, prolonged exposure to bleomycin led to a cycle exit in the G2 phase

(Fig. S5H), documented by complete loss of Ki67 and RB phosphorylation, low RB levels, accumulation of hypo-phosphorylated p130 and G1 cyclins and marked CDK6 (but not CDK4) downregulation (Fig. 5H-left). Notably, G2 exit coincided with further p21 increase concomitant with sustained p53 and Chk2 phosphorylation (Fig. 5H-right). This contrasted with a complete suppression of Chk1 phosphorylation associated with low Chk1 levels, which further highlights differences between the two kinases. Moreover, G2 exit was followed by senescence, as shown by SA-β-gal staining, but this became apparent only after 2-week exposure to genotoxic agents (Fig. 5I and Fig. S5I). Noteworthy, since in U2OS cells INK4A locus is inactivated by methylation (Park et al., 2002), these results suggest that p16 is dispensable for senescence onset.

Thus, sustained Chk1 activity in G2-arrested U2OS cells associates with delayed p21 induction and impaired cell cycle exit, while G2 exit and senescence onset correlate with downregulated Chk1, persistent Chk2 activity and strong accumulation of p21 and G1 cyclins.

Acute Chk1, but not Chk2, depletion promotes DNA damage-induced cell cycle exit by upregulating p21 and inhibiting RB kinases

The striking difference in behaviour between Chk1 and Chk2 suggested that these two kinases might play opposing roles at the onset of G2 exit. Based on our results, and those showing that Chk1 inhibits p21 expression (Beckerman et al., 2009; Hsu et al., 2019) while Chk2 inhibits CDK (Chen and Poon, 2008), we predicted that the Chk1 downregulation should promote DNA damage-induced cell cycle exit, whereas

reduced Chk2 would delay it (Fig. 6A). To test this hypothesis, we knocked down each kinase in U2OS cells, which did not significantly affect cell proliferation (Fig. S6A), before exposure to genotoxic drugs. In agreement with previous work (Bacevic et al., 2017a; Lossaint et al., 2011), Chk1 KD, but not Chk2 KD, abrogated G2 arrest by bleomycin, although, based on FACS results, this was not clear for ICRF-193 (Fig. 6B). Further inspection by video-microscopy showed that the persistence of cells with 4N DNA content upon Chk1 KD in the presence of ICRF-193 was due to accumulation of bi-nucleate G1 cells generated after cytokinesis failure (Fig. 6C).

As predicted, Chk1 depletion potently accelerated DNA damage-induced cell cycle exit (detectable after 16h), as shown by downregulation of Ki67 and CycA, rapid inhibition of CycD1-dependent RB phosphorylation and accumulation of hypo-phosphorylated p130 and G1 cyclins (Fig 6D and Fig. S6B). Consistent with these results, Chk1 KD upregulated p21, stimulated Chk2 phosphorylation, reduced CDK6 levels (Fig. 6D, Fig. S6B), and increased accumulation of p21-bound CycD1-CDK2/4 and CycE1-CDK2 complexes (Fig. 6E). This suggests that Chk1 KD accelerates cell cycle exit by p21-dependent inhibition of RB family kinases as well as by CDK6 downregulation. Strikingly, Chk2 KD produced exactly the opposite effect: increased Ki67, p130/RB phosphorylation and CycA levels, and it did not upregulate G1 cyclins or induce accumulation of p21-bound CycE1 or CycD1 complexes (Fig. 6D, E and Fig. S6B). Notably, Chk2 depletion did not affect p53 phosphorylation on Ser20 (Fig. S6C) nor did it prevent DNA-dependent p21 induction (Fig. 6D), challenging its presumed role in activating p53 (Chen and Poon, 2008; Matthews et al., 2022). In agreement with these

results, Chk2 KD failed to reduce p21 upregulation in HDF treated with ICRF-193, whereas Chk1 KD strongly induced p21 and promoted cell cycle exit even in the absence of DNA damage (Fig. S6D,E). Moreover, Chk1 is not likely to compensate for the absence of Chk2 in activating p53 (Fig. S6C), since p21 induction is not reduced even upon double Chk1/Chk2 knockdown (Fig. S6E). Thus, our results do not support a role for Chk2 in controlling p53 activity in DNA damaged-induced G2 arrest.

Finally, we noticed a marked difference in negative regulation of CDK4 and CDK6 in U2OS cells. Whereas both prolonged DNA damage (Fig. 5H) and Chk1 depletion (Fig. 6D) reduced CDK6, CDK4 levels increased in these situations, accumulating in p21-bound CycD1 complexes (Fig. 6E). To assess respective contributions of CDK4 and CDK6 on RB phosphorylation we knocked down these kinases. Although neither CDK4 KD nor CDK6 KD alone significantly affected CycD-specific RB phosphorylation, it was strongly reduced after double CDK4/6 KD, inhibiting cell cycle progression as documented by downregulation of CDC6 and cyclin B1 (Fig. 6F). These results highlight the importance of CDK6 downregulation in DNA damage-induced cell cycle exit and senescence onset.

Taken together, our data suggest that Chk1 and Chk2 play opposing roles in DNA damage-induced G2 exit/senescence onset in U2OS cells (Fig. 6A). Whereas sustained Chk1 activity stabilizes G2 arrest but antagonises cell cycle exit, possibly by preventing p21-mediated inactivation of RB kinases, Chk2 might promote the latter by preventing RB phosphorylation.

Chk1 knockdown in cancer cells accelerates cell cycle exit by inducing p21 and downregulating CDK6

In U2OS cells, rapid DNA damage-induced cell cycle withdrawal following Chk1 depletion coincided with p21 induction and CDK6 downregulation. We therefore asked whether p21 knockdown would prevent apparition of cell cycle exit hallmarks in Chk1-depleted U2OS cells. To this end, we compared the effects of p21 KD, Chk1 KD and double Chk1/p21 KD (DKD) in non-treated and U2OS cells exposed to bleomycin for 16 or 48 hours.

Unlike Chk1 KD, p21 KD did not abrogate G2 arrest, showing that sustained Chk1 activity can prevent mitosis even after prolonged DNA damage (Fig. 7A and Fig. S7A). In contrast, p21 depletion increased Ki67 levels and p130/RB phosphorylation, abolished G1 cyclin accumulation and supported Chk1 phosphorylation even after prolonged DNA damage (Fig. 7B, and Fig. S7B). Consistent with these results, ATM inhibition by KU-55933 (Ku), which strongly reduced p21 induction and Chk2 activation, did not abrogate G2 arrest but it both increased CycD1-dependent RB phosphorylation and stabilised Chk1 phosphorylation (Fig. 7C and Fig. S7C). In contrast, caffeine, which inhibits both ATR and ATM, abrogated G2 arrest and reduced RB protein and phosphorylation levels (Fig. 7C and Fig. S7C). These results highlight an antagonism between Chk1 activation and ATM/p21/RB-mediated G2 exit. As predicted by our model, Chk1/p21 DKD abolished DNA damage-induced cell cycle exit (Fig. 7B), which resulted in unchecked cell cycle progression, mitotic catastrophe and, ultimately, cell death (Fig. 7A,D and Figs. S7A,D). Moreover, p21 KD counteracted Chk1 KD-mediated

CDK6 downregulation (Fig. 7B, arrowheads), presumably contributing to persistent RB phosphorylation. Thus, our results confirm the key role of p21 in Chk1 KD-induced senescence onset in U2OS cells.

Next, we sought to validate the respective roles of Chk1 and p21 in the onset of G2 exit in another p53/RB-proficient cancer cell line, HCT-116. As with U2OS, RB phosphorylation and Ki67 levels persisted after bleomycin-induced G2 arrest and correlated with sustained Chk1 activation (Fig. 7E and Figs. S7E,F). Chk1 KD abrogated G2 arrest and induced permanent cell cycle exit (low Ki67, unphosphorylated RB), which was associated with upregulation of p21 and G1 cyclins, strong accumulation of p21-bound CycD1-CDK2/CDK4 complexes and CDK6 downregulation (Fig. 7E,F and Fig. S7F). Conversely, while p21 KD failed to abrogate G2 arrest, it increased RB phosphorylation and prevented both CycD1/CycE1 upregulation (Fig. 7F, and Figs. S7E,F) and accumulation of CycD1-CDK complexes (Fig. 7F). Furthermore, consistent with its role in mediating Chk1 KD-induced cell cycle exit, p21 depletion fully restored Ki67, CycA and CDK6 expression, RB phosphorylation (Fig. 7E-8h-DKD) and abolished upregulation of CycE1 and CycD1-CDK complexes (Fig. 7F-DKD). However, after prolonged DNA damage DKD only partially rescued Ki67 expression and RB phosphorylation in HCT-116 cells (Fig. 7E-48 h, asterisk). The latter might be due to upregulation of the CDK inhibitor $p27^{Kip1}$ in CycD1-CDK complexes (Fig. 7F, arrow) and reduced CDK6 levels (Fig. 7E). Moreover, as in U2OS, DKD promoted cell death by abrogating checkpoints and p21-mediated senescence onset (Fig. S7E). Thus, p21 appears to be the main effector mediating DNA damage-induced cell cycle exit after

Chk1 depletion. In addition, our data support the role of sustained Chk1 activation in preventing p21/RB-mediated permanent G2 exit, and corroborate the importance of CDK6 downregulation in senescence onset in cancer cells.

Discussion

Our results reveal that senescence onset upon permanent DNA damage-induced G2 arrest (G2 exit) involves interplay between the p21-cycD-RB pathway and Chk1/Chk2 kinases (Fig. 7G). In non-transformed cells, G2 exit and senescence are triggered by p21-dependent RB activation, which correlates with Chk1 downregulation and precedes the acquisition of senescence hallmarks such as p16 or SA-β-gal. This G2 exit programme is compromised in p53/RB-proficient cancer cells due to inefficient p21-dependent inhibition of RB phosphorylation and sustained Chk1 activation. Acute Chk1 depletion in these cells strongly accelerates cell cycle exit, in p21-dependent manner, by inhibiting or downregulating RB kinases.

We identify CycD1-CDK2/CDK4 complexes as major p21 targets after G2 arrest, thus uncovering their previously unrecognized role in RB phosphorylation in late cell cycle phases (Chung et al., 2019; Topacio et al., 2019). Although often considered, together with $p27^{Kip1}$, as a stabilizer, and even activator, of CycD1-CDK complexes (Sherr and Roberts, 1999), p21 was shown to inhibit CycD1-CDK4 complexes (Guiley et al., 2019; Yang et al., 2017b). Therefore, we propose that p21-CycD1 is an RB-linked DNA damage effector even beyond the G1/S transition, enabling the conversion from a temporary G2 arrest to a permanent G2 exit, which entails senescence onset (Fig. 7G). The presented results are fully consistent with our previous observations (Chassot et al., 2008) and the recent finding that CycD1 also serves as a mitogen sensor, as its

elevated levels in the G2 phase of mother-cells promotes daughter cell proliferation (Min et al., 2020). However, we cannot exclude the possibility that p21 triggers G2 exit by also inhibiting CycA-Cdk2 which phosphorylates RB as well (Topacio et al., 2019).

In addition to its role in blocking G2/M progression, p21 targets CycD1-CDK2 and CycE1-CDK2 complexes, which accumulate upon mitotic bypass, thereby preventing re-replication (Fig. 7G) that might otherwise take place upon APC/C^{Cdh1} inactivation (Cappell et al., 2016). The importance of inhibition of CycD1-CDK2 by p21 is highlighted by the recent discovery that this complex, which efficiently phosphorylates RB (Chytil et al., 2004; Topacio et al., 2019), might confer resistance of cancer cells to CDK4/6 inhibitors such as palbociclib (Chaikovsky et al., 2021; Saengboonmee and Sicinski 2021). Interestingly, p21-bound CycD1/CycE1 complexes strongly accumulate in G2-arrested p53-proficient cancer cells (U2OS, HCT-116) concomitant with CycA downregulation and cell cycle exit, but their function is unclear. We speculate that these complexes, also upregulated after Chk1 depletion and previously observed in "spontaneously" quiescent (Gookin et al, 2017) or senescent (Bacevic et al., 2017a; Stein et al., 1999) cells, might play a role in senescence, for example, by preventing apoptosis.

The notion that p21-RB-mediated Chk1 downregulation promotes permanent cell cycle exit might appear counterintuitive, since sustained Chk1 activity stabilizes G2 arrest, in turn enabling senescence onset (Johmura et al., 2016). Nonetheless, Chk1 suppression has been observed after DNA damage-induced cell cycle arrest or in replicative senescence (Gabai et al., 2008; Gire, 2004; Gottifredi et al., 2001) and implicated in prevention of apoptosis during trophoblast differentiation (Ullah et al.,

2011). Yet, given its key role in DNA damage checkpoints, Chk1 inactivation or downregulation is often regarded as a "defect in the DNA damage response" (Gabai et al., 2008), a mechanism enabling adaptation to genotoxic stress (Shaltiel et al., 2015), recovery from severe replication stress (Zhang et al., 2005), cell cycle resumption after DNA damage repair (Park et al., 2015) or preventing a prolonged G2 arrest which might trigger apoptosis (Gottifredi et al., 2001). In contrast, our results implicate Chk1 downregulation as a necessary component of the senescence programme (Fig. 7G). The observation that telomere dysfunction in the absence of p53 associates with sustained Chk1 activation and endoreplication (Davoli et al., 2010) is fully consistent with our model. Moreover, our results suggest an explanation for the finding that an extra copy of the *Chk1* gene promotes oncogenic transformation in mice (Lopez-Contreras et al., 2012): this might compromise senescence onset and trigger genome instability. There are several potential mechanisms whereby prolonged Chk1 activity enables CDK-mediated RB inactivation and prevents senescence onset. For example, Chk1 might promote cell cycle progression by restraining p21 induction (Beckerman et al., 2009; Hsu et al., 2019), positively regulating CDK6 expression by inhibiting E2F6, a repressor of E2F-dependent transcription (Bertoli et al., 2013) or by phosphorylating and inactivating E2F7 and E2F8, potent transcriptional repressors (Yuan et al., 2018).

Our results showing that DNA damage-induced G2 exit correlates with p53-dependent diminution of γH2AX signal and reduction of γH2AX/53BP1 foci explain the relative absence of γH2AX/53BP1 foci observed in senescent cells (Gire et al., 2004), and could reflect an energy saving switch-off of DNA damage signalling once the cells are committed to permanent cell cycle exit. On the other hand, it is tempting to speculate that

γH2AX/53BP1 foci clustering (Aymard et al., 2017), resembling 53BP1 nuclear bodies (Lukas et al., 2011), might be actively involved in senescence onset (Zhang et al., 2022).

Our finding that prolonged DNA damage or accelerated senescence after Chk1 depletion in cancer cells lacking p16 (Burri et al., 2001; Park et al., 2002) triggers downregulation of CDK6 but not CDK4, not only underlines differential regulation of the two kinases but also uncovers a novel, CDK inhibitor-independent mechanism of inhibiting RB phosphorylation. A nonredundant role for CDK6 in RB phosphorylation is also supported by findings in *Cdk6*$^{-/-}$ mice and our recent study where we found that CDK2 hinders cell cycle exit in part by maintaining CDK6 expression (Bacevic et al., 2017a). Moreover, acquired CDK6 overexpression confers cancer resistance to CDK4/6 (Yang et al., 2017a) and CDK1/2 inhibitors (Bacevic et al., 2017b). Interestingly, CDK6 appears to be less targeted by p21 than CDK4 or CDK2, but upon DNA damage (this study) or in differentiation (Fujimoto et al., 2007) permanent cell cycle arrest correlates with its downregulation. And in replicative senescence, p16-mediated CDK6 sequestration preferentially downregulates CycD1-CDK6 but not CycD1-CDK4 complexes that are p21-bound (Dulic et al., 2000; Stein et al., 1999). This explains why prolonged DNA damage, which entails CDK6 downregulation, promotes senescence in U2OS cells despite the absence of p16.

Perhaps the most surprising result is that acute Chk2 depletion did not affect p53 phosphorylation or p21 induction, which would have been expected from its role as a p53 activator (Chen and Poon, 2008; Matthews et al., 2022) but instead stimulated RB phosphorylation and Ki67 expression in G2-arrested cells. While our present and earlier results (Bacevic et al., 2017a; Lossaint et al., 2011) do not support its presumed but still

debated role in G2 arrest (Stolz et al., 2011), they suggest that Chk2 might promote senescence by inhibiting RB kinases (Fig. 7G). This is consistent with its role in senescence (Chen and Poon, 2008; Gire et al., 2004) and as a global tumour suppressor associated with DNA damage (Stolz et al., 2011; Stracker et al., 2008).

In conclusion, our results support a model where reciprocal regulation of p21 and Chk1 is a core feature of a network that includes both checkpoint (Chk1, Chk2) and senescence (p21 and RB) regulators, and whose combined output controls the fate of G2-arrested cells. Therefore, inhibiting Chk1 in cancers might have therapeutic benefit in combination with genotoxic chemotherapy, as it should promote senescence of cancer cells subjected to DNA damage. As opposed to "synthetic lethality", we propose that "synthetic senescence promotion" would be an appropriate description of such an effect.

Materials and Methods

Cell lines

Normal human diploid foreskin fibroblasts (HDF), HDF expressing HPV16-E6 and human mammary epithelial cells (HMEC), from frozen stocks, were obtained, cultured and synchronized as described previously (Baus et al., 2003; Lossaint et al., 2011). U2OS (human osteosarcoma) cells were originally purchased from ATCC (Manassas, VA, USA) and HCT-116 (colon carcinoma) cells were a gift of Dr. B. Vogelstein (Johns Hopkins University, Baltimore, MD, USA) from 2000 to 2010. The human fibroblasts (BJ) expressing inducible SV40 mutant (T_{121}) specifically targeting pocket proteins (Conklin et al., 2012) were a gift from Dr. J. Sage (Stanford, CA, USA,

in 2018). Cell lines were not authenticated but were weekly tested for mycoplasma contaminations (Mycolalert kit, Basel, Switzerland).

Excepting for HMEC (MEGM medium; Lonza, Basel, Switzerland) and HCT-116 (McCoy's 5A medium, Gibco® Life Technologies, Waltham, MA, USA) all cell lines were cultured in Dulbecco modified Eagle medium (DMEM, high glucose, pyruvate, GlutaMAX – Gibco® Life Technologies, Waltham, MA, USA) supplemented with 10% foetal bovine serum (Sigma-Aldrich, St Louis, MO, USA; Dutcher, Bernolsheim, France or HyClone, Cytiva, Marlborough, MA, USA). Cells were grown under standard conditions at 37°C in humidified incubator containing 5% CO_2.

Cell drug treatments, radiation

Radiomimetic agent bleomycin (Bleomycin sulphate #S1214, Euromedex, Souffelweyersheim, France, 10 µg/ml) and topoisomerase II inhibitor ICRF-193 (bis(2,6-dioxopiperazin)), 2 µg/ml, Sigma-Aldrich, St Louis, MO, USA) were added to asynchronously growing cells as described previously (Baus et al., 2003). Where indicated, cells were irradiated (5 or 10 Gy) in the panoramic ^{60}Co gamma irradiation facility at the Ruđer Bošković Institute (Zagreb, Croatia; (Majer et al., 2019). Caffeine (SA, 5 mM) and ATM inhibitor KU-0055933 (Kudos Pharmaceuticals, Cambridge, UK, 10 µM) were added 1 hr before treatment with drugs. Doxycycline (ThermoFisher, Waltham, MA, USA) was added 6-12 hr before adding the genotoxic drugs (1 µg/ml).

Cell cycle analysis

Cell cycle analysis was determined by flow cytometry (FACS) of propidium iodide (PI)-stained cells using BD FACS Calibur (BD Biosciences, San Jose, CA, USA) as described earlier (Bacevic et al., 2017a). Cells were harvested, washed with cold PBS, resuspended in 300 µL PBS and fixed with 700 µL ice-cold 100% methanol. Fixed cells were kept at -20°C. For the analysis, cells were pelleted by centrifugation at 6000 rpm for 5 min. After washing once with 1% BSA in PBS, cells were stained with PI staining solution (10 µg/ml PI, 1% BSA, 200 µg/ml RNase A in PBS) for 15 min at room temperature and subjected to cell cycle analysis using BD FACS Calibur (BD Biosciences, San Jose, CA). Data were analysed using FlowJo software (v10.6.1, FlowJo, LLC, Ashland, OR, USA).

siRNA transfection

The SMARTpool ON-TARGETplus siRNAs (CHK1, CHK2, CDK2, CDK4, CDK6 or CDKN1A-p21) were purchased from GE Dharmacon Research (Lafayette, CO, USA). As control, we used siRNA for luciferase, 5′- ACUGACGACUCUGCUACUC-3′ (Luc; Eurogentec, Seraing, Belgium) or ON-TARGETplus Non-targeting siRNA #1 (Cont; GE Dharmacon). Cells were transfected with siRNA (40 nM) using a standard calcium phosphate transfection method (Bacevic et al., 2017a). 24 hr after transfection, the cells were exposed to genotoxic agents for indicated times and harvested for biochemical or immunofluorescence analysis or monitored by video-microscopy (Lossaint et al., 2011).

Preparation of cell lysates and conditions for SDS-PAGE and immunoblotting have been described previously (Baus et al., 2003; Stein et al., 1999). Briefly, cells were harvested by trypsinisation and washed in cold PBS prior freezing in liquid N_2. Frozen pellets (kept at -80°C) were lysed in lysis buffer (150 mM NaCl, 50 mM Tris-HCl pH 7.5, 0.2% NP-40, 2 mM EDTA, 1 mM DTT, 0.1 mM $NaVO_4$, protease inhibitor cocktail (Sigma Aldrich, P 8340) and incubated on ice (60 min). Lysates were centrifuged at 13,000 rpm (5 min) and supernatant was frozen (80°C). Total protein was quantified using the BCA Protein Assay Kit (Pierce Biotechnology; ThermoFisher, #23227). For immunoblot analysis, cell lysates were denatured in Laemmli buffer and boiled at 95°C for 5 min. 30 µg of protein was loaded into each lane. Samples were run on 7.5%, 11% or 12.5% SDS-PAGE gels, depending on the proteins of interest, and transferred to Immobilon membranes (Merck Millipore, Burlington, MA, USA) using Owl HEP-1 semidry electroblotter (ThermoFisher). Membranes were routinely stained with Naphtol blue black (Amido-black; Sigma-Aldrich, 3393) to verify the transfer and loading. Primary antibodies were diluted in 5% milk in TBS-T and incubated for 2 hr at RT or overnight at 4°C. Secondary antibodies (goat anti-mouse IgG-HRP, DACO, Glostrup, Denmark and donkey anti-rabbit IgG-HRP, GE Healthcare, Chicago, IL, USA) were diluted 1:5000 in 5% milk in TBS-T and incubated for 1 hr at room temperature. Chemiluminescence was detected using Western Lightning Plus/Ultra (PerkinElmer, Villebon sur Yvette, France) and Amersham Hyperfilm™ (GE Healthcare, Chicago, IL, USA).

Antibodies

Primary antibodies for western blotting: cyclin D1 (Santa Cruz Biotechnology (SCBT), Dallas, TX, USA DCS-6, sc-20044), cyclin D2 (SCBT, sc-593), cyclin D3 (SCBT, sc-182), cyclin E1 (SCBT, sc-247), cyclin A (Novocastra Laboratories Ltd., Newcastle upon Tyne, UK, 6E6) , cyclin B1 (SCBT, sc-752; 1:100), CDK1 (BD Transduction Laboratories (BDTL), San Jose, CA, USA, C12720), CDK2 (Abcam, Cambridge, UK, ab128167), CDK4 (SCBT, sc-260; 1:1000), CDK6 (SCBT, sc-177), p16 (BD Pharmingen, San Diego, CA, USA, 550834; 1:100), p21 (SCBT, sc-397 and Cell Signaling Technology (CST), Danvers, MA, USA, 2946, 2947), p27 (SCBT, sc-528; and BDTL , K25020), RB (BD Pharmingen, 554136; 1:200), p130 (SCBT, sc-317; 1:200), RB phospho-S780 (CST, 9307), Chk1 (SCBT sc-8408), Chk2 (SCBT, sc-17747), Chk1 phospho-S317 (CST, 12302), Chk1 phospho-S345 (CST, 2348), Chk2 phospho-T68 (CST, 2661), Cdc25C phospho-S216 (CST, 4901), p53 (SCBT, sc-126), p53 phospho-S15 (CST, 9284), Ki-67 (Abcam, ab16667). Dilutions were 1:500 or 1:200 for phospho-proteins, unless otherwise specified. For more details see Supplementary information for antibodies.

Co-immunoprecipitation, p21 immuno-depletion

Cells were lysed as described above. Routinely, 100-200 μg of total cell protein was used per IP and antibody against target protein was added at a concentration of 4 μg antibody/mg of total protein, unless otherwise specified. Samples were incubated with the primary antibody for 2 hr at 4°C and the immuno-complexes were recovered using Protein A or Protein G Sepharose beads (Amersham Biosciences, Piscataway, NJ,

USA, 10 μl/100 μl of lysates). Beads were washed in TBS-T, and immunoprecipitated proteins were eluted in 2x Laemmli buffer by heating at 37°C for 15 min. To detect proteins on immunoblots containing immunoprecipitates peroxidase-conjugated protein A/G was used (Pierce Biotechnology, Rockford, IL, USA, 32490). Primary antibodies for immunoprecipitations: cyclin E1 (SCBT, sc-248), p21 (SCBT, sc-397), p27 (SCBT, sc-528) and rabbit polyclonal anti-cyclin D1 (Dulic et al., 1993, 1 μl/100 μl of lysate). For more details see Supplementary information for antibodies.

For p21 or p27 immunodepletion experiments, cell lysates (100-200 μg) were incubated with saturating amounts of p21 or p27 antibodies, whereas mock samples were incubated with protein A-Sepharose only. The resulting supernatants were analysed by immunoblotting as described previously (Stein et al., 1999).

Immunofluorescence, image analysis

Experimental conditions for immunofluorescence, primary antibodies and image analysis (image acquisition and analysis) have been published previously (Bacevic et al., 2017a; Lossaint et al., 2011). Briefly, cells were seeded on coverslips and fixed in cold 100% methanol (10 min, -20°C) or formaldehyde (3.7%, 15 min, RT). Prior to incubation with primary antibodies (1-2 hr at RT in humidified chamber) formaldehyde-fixed cells were permeabilized in 0.2% Triton X-100. Primary and secondary antibodies were diluted in blocking solution (0.1% Tween-20 in PBS with 5% FCS, 2 hr, RT). After washing in PBS-Tween (3 times for 5 min) the cells were incubated with secondary antibody (1 hr at RT) and washed again (3 times for 5 min). Secondary antibodies were

diluted 1:1000 for fluorophores AlexaFluor 488, 555, and 568, and 1:500 for AlexaFluor 647 (Invitrogen, Fisher Scientific). Coverslips were rinsed in distilled water prior to mounting on slide with ProLong Diamond Antifade Mountant with DAPI (Molecular Probes, Eugene, OR, USA, P36962). Immunofluorescence images were captured on microscope Leica CTR6000 (objective Leica 40X HCX PL APO 1.25-0.75 oil, camera CollSnap HQ2, Wetzlar, Germany) driven by MetaMorph (MDS, Analytical Technologies, Canada). Composites were generated using Adobe Photoshop (Adobe systems, Inc, San Jose, CA, USA) and Microsoft PowerPoint (Microsoft Corp, Redmond, WA, USA) softwares. For the panels showing immunofluorescence images, a representative field was shown.

Following primary antibodies were used: cyclin E1 (HE12, SCBT, sc-247; 1:100), cyclin D1 (CST, 2926; Abcam ab16663), cyclin A (Novocastra, 6E6 and SCBT sc751), cyclin B1 (SCBT, sc-752; 1:100), p21 (CST, 2946, 2947), H2A.X phospho-S139 (Merck Millipore, clone JBW301, 05-636), 53BP1 (Novus biologicals, Littleton, CO, USA, NB100-304); Ki-67 (Abcam, ab16667 and BDTL, 610968). Dilutions were 1:500 unless otherwise specified. For more details see Supplementary information for antibodies.

Every experiment was performed at least twice with each genotoxic agent. For each condition, at least ten images (40X magnification) were taken with a widefield fluorescent microscope for each situation. Immunofluorescence signals were quantified using a custom script in ImageJ software (Virginie Georget, MRI) as described previously (Bacevic et al., 2017a). DAPI images were used to identify the individual nuclei using a background correction, a mask creation based on threshold, watershed

segmentation and the "analyse particles" function in ImageJ. The region-of-interest corresponding to the nuclei were applied to the different channels and total intensity of individual nuclei was quantified. The boxplots from quantification data were generated with R (version 3.6.2) and represent cell pools of at least two independent experiments. For the panels showing immunofluorescence images, representative fields were shown.

Video-microscopy

Conditions for video-microscopy were described previously (Bacevic et al., 2017a; Lossaint et al., 2011). Mitoses were scored by inspection of video-microscopy sequences (MetaMorph software). Images were taken at 10-15 min intervals for at least 48 hours. Three fields for each situation were analysed and normalized for the cell number at the beginning of the time-lapse sequence. For mitosis-entry kinetics, total number of mitotic cells during the given interval was plotted. For each experiment, all the conditions were tested in parallel, including controls with untreated cells transfected with different siRNAs.

SA-β-galactosidase

Conditions for SA-β-galactosidase staining using Senescence detection kit (Abcam, ab655351) were described previously (Bacevic et al., 2017a; Sobecki et al., 2017). HDF or U2OS cells were seeded on coverslips in 12-well plate, at density of 10^5 cells per well. After 24 hr, cells were treated with ICRF-193 (2 µg/ml) or bleomycin (10

μg/ml). The drug was washed away from the cells after 48 hr incubation, followed by staining after 2 or 4 weeks using Senescence detection kit (Abcam, ab655351). Photos were taken using an upright microscope at 20X magnification.

Statistical analysis

Each experiment was performed independently two to three times. Data are presented as the mean ± standard deviation (SD) or standard error of mean (SEM) . The two-sided Student's *t*-test was performed using Microsoft® Excel® 2016 (Microsoft Corp, Redmond, WA, USA) to analyse the differences between the means of groups. Differences were considered statistically significant for a p value of ≤ 0.05 labelled by an asterisk (*). Immunofluorescent images were quantified using ImageJ software. Box plots and violin plots were generated using R software. For all analyses, the cells were pooled from two to three independent experiments and at least 200 cells were analysed.

Acknowledgements

This work was supported by Fondation ARC pour la recherche sur le cancer (N°3793 to V.D.) and the Cancéropole du Grand Sud Ouest. The team (GL, KB, VD, KM and DF) is "Equipe labellisé" by the Ligue Nationale Contre le Cancer (EL2013.LNCC/DF). GL and KB were recipients of a PhD fellowship from LNCC. A.H. was funded by Croatian Science Foundation (grant IP-2013-11-1615). V. Gire was funded by Institut national du cancer (INCA) 2017-169. We are grateful to KUDOS Pharmaceuticals for gift of KU-

55933 and Dr. Julien Sage (Stanford, USA) for generous gift of T_{121}-expressing fibroblasts. We thank Dr. Annick Péléraux for statistical analysis of immunofluorescence images and the figures using R software. We thank Drs Etienne Schwob, Alain Camasses, Jacques Piette, Julien Sage and Philippe Coulombe for critically reading various versions of the manuscript. We acknowledge the imaging facility Montpellier Ressources Imagerie (MRI), member of the national infrastructure France-BioImaging supported by the French National Research Agency (ANR-10-INBS-04, «Investments for the future»).

Author Contributions

VD, GL and AH designed research, GL, AH, VGi, KB, VD and KM performed the experiments. VGe created ImageJ macros for immunofluorescence image quantifications. VD and DF wrote the manuscript. All authors reviewed the manuscript.

Conflict of interest Statement

The authors declare that they have no conflict of interest.

References:

Alcorta, D. A., Xiong, Y., Phelps, D., Hannon, G., Beach, D. and Barrett, J. C. (1996). Involvement of the cyclin-dependent kinase inhibitor p16 (INK4a) in replicative senescence of normal human fibroblasts. *Proc Natl Acad Sci U S A* **93**, 13742-7.

Aymard, F., Aguirrebengoa, M., Guillou, E., Javierre, B. M., Bugler, B., Arnould, C., Rocher, V., Iacovoni, J. S., Biernacka, A., Skrzypczak, M. et al. (2017). Genome wide mapping of long range contacts unveils DNA Double Strand Breaks clustering at damaged active genes. *Nat Struct Mol Biol* **24**, 353–361.

Bacevic, K., Lossaint, G., Achour, T. N., Georget, V., Fisher, D. and Dulic, V. (2017a). Cdk2 strengthens the intra-S checkpoint and counteracts cell cycle exit induced by DNA damage. *Sci Rep* **7**, 13429.

Bacevic, K., Noble, R., Soffar, A., Wael Ammar, O., Boszonyik, B., Prieto, S., Vincent, C., Hochberg, M. E., Krasinska, L. and Fisher, D. (2017b). Spatial competition constrains resistance to targeted cancer therapy. *Nat Commun* **8**, 1995.

Baus, F., Gire, V., Fisher, D., Piette, J. and Dulic, V. (2003). Permanent cell cycle exit in G2 phase after DNA damage in normal human fibroblasts. *Embo J* **22**, 3992-4002.

Beckerman, R., Donner, A. J., Mattia, M., Peart, M. J., Manley, J. L., Espinosa, J. M. and Prives, C. (2009). A role for Chk1 in blocking transcriptional elongation of p21 RNA during the S-phase checkpoint. *Genes Dev* **23**, 1364-77.

Bertoli, C., Klier, S., McGowan, C., Wittenberg, C. and de Bruin, R. A. (2013). Chk1 inhibits E2F6 repressor function in response to replication stress to maintain cell-cycle transcription. *Curr Biol* **23**, 1629-37.

Broude, E. V., Swift, M. E., Vivo, C., Chang, B. D., Davis, B. M., Kalurupalle, S., Blagosklonny, M. V. and Roninson, I. B. (2007). p21(Waf1/Cip1/Sdi1) mediates retinoblastoma protein degradation. *Oncogene* **26**, 6954-8.

Bunz, F., Dutriaux, A., Lengauer, C., Waldman, T., Zhou, S., Brown, J. P., Sedivy, J. M., Kinzler, K. W. and Vogelstein, B. (1998). Requirement for p53 and p21 to sustain G2 arrest after DNA damage. *Science* **282**, 1497-501.

Burri, N., Shaw, P., Bouzourene, H., Sordat, I., Sordat, B., Gillet, M., Schorderet, D., Bosman, F. T. and Chaubert, P. (2001). Methylation Silencing and Mutations of the p14ARF and p16INK4a Genes in Colon Cancer. *Lab Invest* **81**, 217-229.

Cappell, S. D., Chung, M., Jaimovich, A., Spencer, S. L. and Meyer, T. (2016). Irreversible APC(Cdh1) Inactivation Underlies the Point of No Return for Cell-Cycle Entry. *Cell* **166**, 167-80.

Chaikovsky, A. C., Li, C., Jeng, E. E., Loebell, S., Lee, M. C., Murray, C. W., Cheng, R., Demeter, J., Swaney, D. L., Chen, S. H. et al. (2021). The AMBRA1 E3 ligase adaptor regulates the stability of cyclin D. *Nature* **592**, 794–798.

Charrier-Savournin, F. B., Chateau, M. T., Gire, V., Sedivy, J., Piette, J. and Dulic, V. (2004). p21-Mediated nuclear retention of cyclin B1-Cdk1 in response to genotoxic stress. *Mol Biol Cell* **15**, 3965-76.

Chassot, A. A., Lossaint, G., Turchi, L., Meneguzzi, G., Fisher, D., Ponzio, G. and Dulic, V. (2008). Confluence-induced cell cycle exit involves pre-mitotic CDK inhibition by p27(Kip1) and cyclin D1 downregulation. *Cell Cycle* **7**, 2038-46.

Chen, J. Y., Lin, J. R., Tsai, F. C. and Meyer, T. (2013). Dosage of Dyrk1a Shifts Cells within a p21-Cyclin D1 Signaling Map to Control the Decision to Enter the Cell Cycle. *Mol Cell* **52**, 87-100.

Chen, Y. and Poon, R. Y. (2008). The multiple checkpoint functions of CHK1 and CHK2 in maintenance of genome stability. *Front Biosci* **13**, 5016-29.

Chicas, A., Wang, X., Zhang, C., McCurrach, M., Zhao, Z., Mert, O., Dickins, R. A., Narita, M., Zhang, M. and Lowe, S. W. (2010). Dissecting the unique role of the retinoblastoma tumor suppressor during cellular senescence. *Cancer Cell* **17**, 376-87.

Chowdhury, D., Keogh, M. C., Ishii, H., Peterson, C. L., Buratowski, C. and Lieberman, J. (2005). gamma-H2AX dephosphorylation by protein phosphatase 2A facilitates DNA double-strand break repair. *Mol Cell* **20**, 801-809.

Chung, M., Liu, C., Yang, H. W., Koberlin, M. S., Cappell, S. D. and Meyer, T. (2019). Transient Hysteresis in CDK4/6 Activity Underlies Passage of the Restriction Point in G1. *Mol Cell* **76**, 562-573 e4.

Chytil, A., Waltner-Law, M., West, R., Friedman, D., Aakre, M., Barker, D. and Law, B. (2004). Construction of a cyclin D1-Cdk2 fusion protein to model the biological functions of cyclin D1-Cdk2 complexes. *J Biol Chem* **279**, 47688-98.

Conklin, J. F., Baker, J. and Sage, J. (2012). The RB family is required for the self-renewal and survival of human embryonic stem cells. *Nat Commun* **3**, 1244.

Davoli, T. and de Lange, T. (2012). Telomere-driven tetraploidization occurs in human cells undergoing crisis and promotes transformation of mouse cells. *Cancer Cell* **21**, 765-76.

Davoli, T., Denchi, E. L. and de Lange, T. (2010). Persistent telomere damage induces bypass of mitosis and tetraploidy. *Cell* **141**, 81-93.

Di Micco, R., Krizhanovsky, V., Baker, D. and Fagagna, F. d. A. d. (2021). Cellular senescence in ageing: from mechanisms to therapeutic opportunities. *Nat Rev Mol Cell Biol* **22**, 75-95.

Dulic, V., Beney, G. E., Frebourg, G., Drullinger, L. F. and Stein, G. H. (2000). Uncoupling between phenotypic senescence and cell cycle arrest in aging p21-deficient fibroblasts. *Mol Cell Biol* **20**, 6741-6754.

Dulic, V., Drullinger, L. F., Lees, E., Reed, S. I. and Stein, G. H. (1993). Altered regulation of G1 cyclins in senescent human diploid fibroblasts: accumulation of inactive cyclin E-Cdk2 and cyclin D1-Cdk2 complexes. *Proc Natl Acad Sci U S A* **90**, 11034-8.

Feringa, F. M., Raaijmakers, J. A., Hadders, M. A., Vaarting, C., Macurek, L., Heitink, L., Krenning, L. and Medema, R. H. (2018). Persistent repair intermediates induce senescence. *Nat Commun* **9**, 3923.

Fujimoto, T., Anderson, K., Jacobsen, S. E., Nishikawa, S. I. and Nerlov, C. (2007). Cdk6 blocks myeloid differentiation by interfering with Runx1 DNA binding and Runx1-C/EBPalpha interaction. *Embo J* **26**, 2361-70.

Gabai, V. L., O'Callaghan-Sunol, C., Meng, L., Sherman, M. Y. and Yaglom, J. (2008). Triggering senescence programs suppresses Chk1 kinase and sensitizes cells to genotoxic stresses. *Cancer Res* **68**, 1834-42.

Geng, Y., Yu, Q., Sicinska, E., Das, M., Bronson, R. T. and Sicinski, P. (2001). Deletion of the p27Kip1 gene restores normal development in cyclin D1-deficient mice

Y Geng et al. . *Proc Natl Acad Sci U S A* **98**, 94-99.

Gire, V. (2004). Dysfunctional Telomeres at Senescence Signal Cell Cycle Arrest via Chk2. *Cell Cycle* **3**, 1217-1220.

Gire, V. and Dulic, V. (2015). Senescence from G2 arrest, revisited. *Cell Cycle* **14**, 297-304.

Gire, V., Roux, P., Wynford-Thomas, D., Brondello, J. M. and Dulic, V. (2004). DNA damage checkpoint kinase Chk2 triggers replicative senescence. *Embo J* **23**, 2554-63.

Gookin, S., Min, M., Phadke, H., Chung, M., Moser, J., Miller, I., Carter, D. and Spencer, S. L. (2017). A map of protein dynamics during cell-cycle progression and cell-cycle exit. *PLoS Biol* **15**, e2003268.

Gottifredi, V., Karni-Schmidt, O., Shieh, S. S. and Prives, C. (2001). p53 down-regulates CHK1 through p21 and the retinoblastoma protein. *Mol Cell Biol* **21**, 1066-76.

Guiley, K. Z., Stevenson, J. W., Lou, K., Barkovich, K. J., Kumarasamy, V., Wijeratne, T. U., Bunch, K. L., Tripathi, S., Knudsen, E. S., Witkiewicz, A. K. et al. (2019). p27 allosterically activates cyclin-dependent kinase 4 and antagonizes palbociclib inhibition. *Science* **366**.

He, S. and Sharpless, N. E. (2017). Senescence in Health and Disease. *Cell* **169**, 1000-1011.

Herbig, U., Jobling, W. A., Chen, B. P., Chen, D. J. and Sedivy, J. M. (2004). Telomere shortening triggers senescence of human cells through a pathway involving ATM, p53, and p21(CIP1), but not p16(INK4a). *Mol Cell* **14**, 501-13.

Hitomi, M. and Stacey, D. W. (1999). Cyclin D1 production in cycling cells depends on ras in a cell-cycle- specific manner. *Curr Biol* **9**, 1075-84.

Hsu, C.-H., Altschuler, S. J. and Wu, L. W. (2019). Patterns of Early p21 Dynamics Determine Proliferation-Senescence Cell Fate after Chemotherapy. *Cell* **178**, 361-371.

Ito, T., Teo, Y. V., Evans, S. A., Neretti, N. and Sedivy, J. M. (2018). Regulation of Cellular Senescence by Polycomb Chromatin Modifiers through Distinct DNA Damage- and Histone Methylation-Dependent Pathways. *Cell Rep* **22**, 3480-3492.

Jackson, M. W., Agarwal, M. K., Yang, J., Bruss, P., Uchiumi, T., Agarwal, M. L., Stark, G. R. and Taylor, W. R. (2005). p130/p107/p105Rb-dependent transcriptional repression during DNA-damage-induced cell-cycle exit at G2. *J Cell Sci* **118**, 1821-32.

Johmura, Y., Shimada, M., Misaki, T., Naiki-Ito, A., Miyoshi, H., Motoyama, N., Ohtani, N., Hara, E., Nakamura, M., Morita, A. et al. (2014). Necessary and sufficient role for a mitosis skip in senescence induction. *Mol Cell* **55**, 73-84.

Johmura, Y., Yamashita, E., Shimada, M., Nakanishi, K. and Nakanishi, M. (2016). Defective DNA repair increases susceptibility to senescence through extension of Chk1-mediated G2 checkpoint activation. *Sci Rep* **6**, 31194.

Kitagawa, M., Higashi, H., Jung, H. K., Suzuki-Takahashi, I., Ikeda, M., Tamai, K., Kato, J., Segawa, K., Yoshida, E., Nishimura, S. et al. (1996). The consensus motif for phosphorylation by cyclin D1-Cdk4 is different from that for phosphorylation by cyclin A/E-Cdk2. *Embo J* **15**, 7060-7069.

Kleiblova, P., Shaltiel, I. A., Benada, J., Sevcik, J., Pechackova, S., Pohlreich, P., Voest, E. E., Dundr, P., Bartek, J., Kleibl, Z. et al. (2013). Gain-of-function mutations of PPM1D/Wip1 impair the p53-dependent G1 checkpoint. *J Cell Biol* **201**, 511-21.

Krenning, L., Feringa, F. M., Shaltiel, I. A., van den Berg, J. and Medema, R. H. (2014). Transient activation of p53 in G2 phase is sufficient to induce senescence. *Mol Cell* **55**, 59-72.

Lemmens, B. and Lindqvist, A. (2019). DNA replication and mitotic entry: A brake model for cell cycle progression *J Cell Biol* **218** 3892–3902.

Lobrich, M. and Jeggo, P. A. (2007). The impact of a negligent G2/M checkpoint on genomic instability and cancer induction. *Nat Rev Cancer* **7**, 861-9.

Lopez-Contreras, A. J., Gutierrez-Martinez, P., Specks, J., Rodrigo-Perez, S. and Fernandez-Capetillo, O. (2012). An extra allele of Chk1 limits oncogene-induced replicative stress and promotes transformation. *J Exp Med* **209**, 455-61.

Lossaint, G., Besnard, E., Fisher, D., Piette, J. and Dulic, V. (2011). Chk1 is dispensable for G2 arrest in response to sustained DNA damage when the ATM/p53/p21 pathway is functional. *Oncogene* **30**, 4261-74.

Lukas, C., Savic, V., Bekker-Jensen, S., Doil, C., Neumann, B., Pedersen, R. S., Grofte, M., Chan, K. L., Hickson, I. D., Bartek, J. et al. (2011). 53BP1 nuclear bodies form around DNA lesions generated by mitotic transmission of chromosomes under replication stress. *Nat Cell Biol* **13**, 243-53.

Lundberg, A. S. and Weinberg, R. A. (1998). Functional inactivation of the retinoblastoma protein requires sequential modification by at least two distinct cyclin-cdk complexes. *Mol Cell Biol* **18**, 753-61.

Macurek, L., Lindqvist, A., Voets, O., Kool, J., Vos, H. R. and Medema, R. H. (2010). Wip1 phosphatase is associated with chromatin and dephosphorylates gammaH2AX to promote checkpoint inhibition. *Oncogene* **29**, 2281-91.

Majer, M., Roguljić, M., Knežević, Ž., Starodumov, A., Ferenček, D., Brigljević, V. and Mihaljević, B. (2019). Dose mapping of the panoramic 60Co gamma irradiation facility at the Ruđer Bošković Institute
– Geant4 simulation and measurements. *Appl. Radiat. Isot.* **154**, 108824.

Matsushime, H., Quelle, D. E., Shurtleff, S. A., Shibuya, M., Sherr, C. J. and Kato, J. Y. (1994). D-type cyclin-dependent kinase activity in mammalian cells. *Mol. Cell. Biol.* **14**, 2066-2076.

Matthews, H. M., Bertoli, C. and de Bruin, R. A. (2022). Cell cycle control in cancer. *Nat Rev Mol Cell Biol* **23**, 74-88.

Min, M., Rong, Y., Tian, C. and Spencer, S. (2020). Temporal integration of mitogen history in mother cells controls proliferation of daughter cells. *Science* **368**, 1261-1265.

Park, C., Suh, Y. and Cuervo, A. M. (2015). Regulated degradation of Chk1 by chaperone-mediated autophagy in response to DNA damage. *Nat Commun* **6**, 6823.

Park, Y.-B., Park, M. J., Kimura, K., Shimizu, K., Lee, S. H. and Yokota, J. (2002). Alterations in the INK4a/ARF locus and their effects on the growth of human osteosarcoma cell lines. *Cancer Genet Cytogenet.* **133**, 105-111.

Roger, L., Tomas, F. and Gire, V. (2021). Mechanisms and Regulation of Cellular Senescence. *Int J Mol Sci.* **22**, 13173.

Sadasivam, S. and DeCaprio, J. A. (2013). The DREAM complex: master coordinator of cell cycle-dependent gene expression. *Nat Rev Cancer* **13**, 585-95.

Saengboonmee, C. and Sicinski , P. (2021). The path to destruction for D-type cyclin proteins. *Nature* **592**, 690-691.

Shaltiel, I. A., Krenning, L., Bruinsma, W. and Medema, R. H. (2015). The same, only different - DNA damage checkpoints and their reversal throughout the cell cycle. *J Cell Sci* **128**, 607-20.

Sharpless, N. E. and Sherr, C. J. (2015). Forging a signature of in vivo senescence. *Nat Rev Cancer* **15**, 397-408.

Sherr, C. J. and Roberts, J. M. (1999). CDK inhibitors: positive and negative regulators of G1-phase progression. *Genes Dev* **13**, 1501-12.

Sobecki, M., Mrouj, K., Colinge, J., Gerbe, F., Jay, P., Krasinska, L., Dulic, V. and Fisher, D. (2017). Cell-Cycle Regulation Accounts for Variability in Ki-67 Expression Levels. *Cancer Res* **77**, 2722-2734.

Stein, G. H., Drullinger, L. F., Soulard, A. and Dulic, V. (1999). Differential roles for cyclin-dependent kinase inhibitors p21 and p16 in the mechanisms of senescence and differentiation in human fibroblasts. *Mol Cell Biol* **19**, 2109-17.

Stolz, A., Ertych, N. and Bastians, H. (2011). Tumor suppressor CHK2: regulator of DNA damage response and mediator of chromosomal stability. *Clin Cancer Res* **17**, 401-5.

Stracker, T. H., Couto, S. S., Cordon-Cardo, C., Matos, T. and Petrini, J. H. (2008). Chk2 suppresses the oncogenic potential of DNA replication-associated DNA damage. *Mol Cell* **31**, 21-32.

Sturmlechner, I., Zhang, C., Sine, C. C., van Deursen, E.-J., Jeganathan, K. B., Hamada, N., Grasic, J., Friedman, D., Stutchman, J. T., Can, I. et al. (2021). p21 produces a bioactive secretome that places stressed cells under immunosurveillance. *Science* **374**, 577-581.

Topacio, B. R., Zatulovskiy, E., Cristea, S., Xie, S., Tambo, C. S., Rubin, S. M., Sage, J., Kõivomägi, M. and Skotheim, J. M. (2019). Cyclin D-Cdk4,6 Drives Cell-Cycle Progression via the Retinoblastoma Protein's C-Terminal Helix . *Mol Cell* **74**, 758-770.

Ullah, Z., de Renty, C. and DePamphilis, M. L. (2011). Checkpoint kinase 1 prevents cell cycle exit linked to terminal cell differentiation. *Mol Cell Biol* **31**, 4129-43.

Yang, C., Li, Z., Bhatt, T., Dickler, M., Giri, D., Scaltriti, M., Baselga, J., Rosen, N. and Chandarlapaty, S. (2017a). Acquired CDK6 amplification promotes breast cancer resistance to CDK4/6 inhibitors and loss of ER signaling and dependence. *Oncogene* **36**, 2255-2264.

Yang, H. W., Chung, M., Kudo, T. and Meyer, T. (2017b). Competing memories of mitogen and p53 signalling control cell-cycle entry. *Nature* **549**, 404-408.

Yang, K., Hitomi, M. and Stacey, D. W. (2006). Variations in cyclin D1 levels through the cell cycle determine the proliferative fate of a cell. *Cell Div* **1**, 32.

Yosef, R., Pilpel, N., Papismadov, N., Gal, H., Ovadya, Y., Vadai, E., Miller, S., Porat, Z., Ben-Dor, S. and Krizhanovsky, V. (2017). p21 maintains senescent cell viability under persistent DNA damage response by restraining JNK and caspase signaling. *Embo J* **36**, 2280-2295.

Yuan, R., Vos, H. R., van Es, R. M., Chen, J., Burgering, B. M., Westendorp, B. and de Bruin, A. (2018). Chk1 and 14-3-3 proteins inhibit atypical E2Fs to prevent a permanent cell cycle arrest. *Embo J* **37**.

Zhang, L., Geng, X., Wang, F., Tang, J., Ichida, Y., Sharma, A., Jin, S., Chen, M., Tang, M., Pozo, F. M. et al. (2022). 53BP1 regulates heterochromatin through liquid phase separation. *Nat Commun* **13**, 360.

Zhang, Y. W., Otterness, D. M., Chiang, G. G., Xie, W., Liu, Y. C., Mercurio, F. and Abraham, R. T. (2005). Genotoxic stress targets human Chk1 for degradation by the ubiquitin-proteasome pathway. *Mol Cell* **19**, 607-18.

Figures

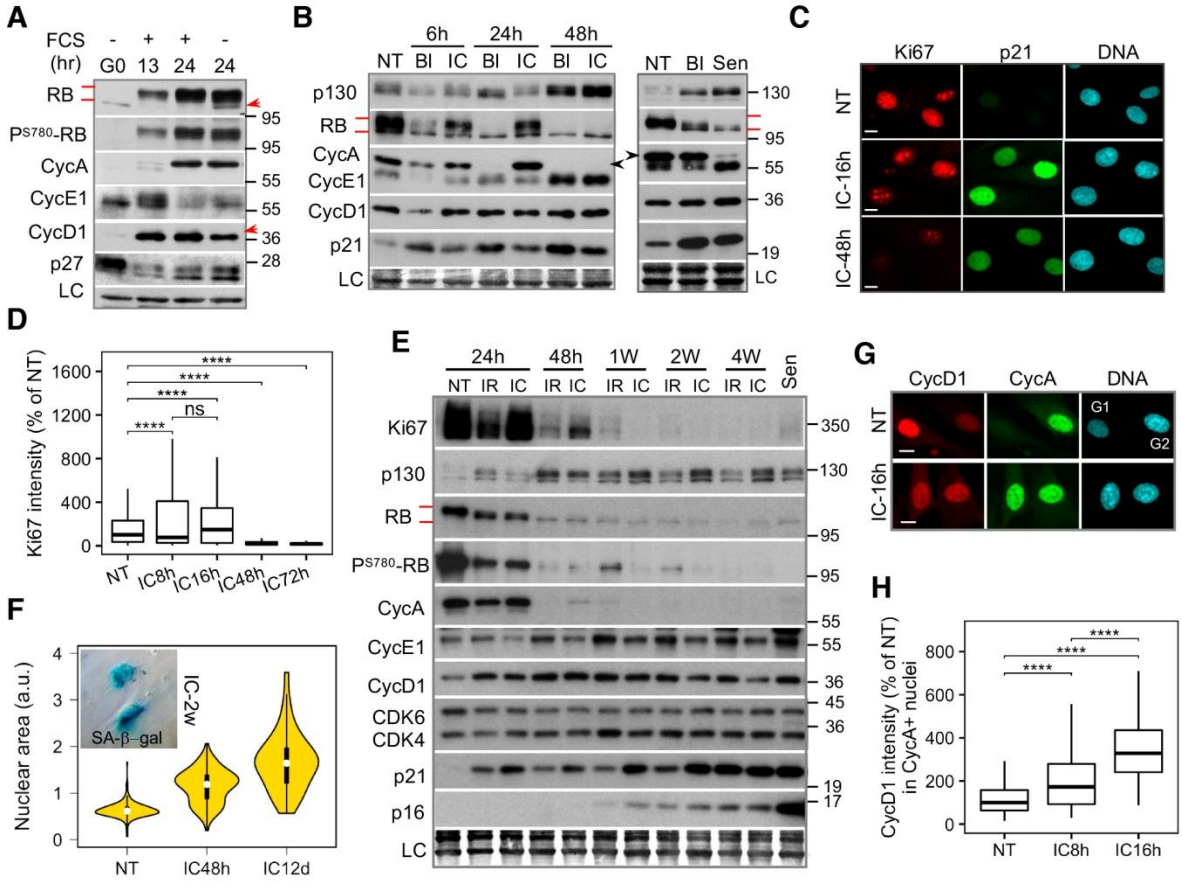

Fig. 1. CycD1 and CycE1 accumulate upon DNA damage-induced G2 arrest prior to cell cycle exit and senescence

A. Immunoblots showing RB levels, CycD1-specific phosphorylation (P^{S780}-RB) and expression of different cyclins in HDF released from quiescence (G0) by serum addition (+FCS). For 24h- timepoint FCS was removed after 13h. Red arrows indicate hypo-phosphorylated RB and reduced CycD1 levels in the absence of FCS. LC, loading control.

B. Immunoblots showing cyclins, p21, RB and p130 after DNA damage-induced cell cycle exit (left panel) and in HDF that underwent replicative senescence (Sen, right panel). HDF were incubated with bleomycin (Bl) or ICRF-193 (IC) for indicated times (left panel) and for 12 hr (right panel). Sen: population doubling (PD) 74. NT, non-treated cells. Arrows show CycA band. LC, loading control.

C. Representative immunofluorescence images showing co-expression of Ki67 and p21 in non-treated (NT) and HDF incubated with ICRF-193 (IC) for 16 and 48 hours (n=3). Scale bar, 10 μM.

D. Quantification of Ki67 intensity in immunofluorescence images from HDF incubated with ICRF-193 (IC) for indicated times (% of NT). Pooled cells from four independent experiments. More than 100 cells were analysed in each experiment. NT, non-treated cells. Box plot whiskers indicate 10-90% boundary. ns, not significant.

E. Immunoblots showing changes in indicated cell cycle regulators, RB levels and CycD1-specific phosphorylation (P^{S780}-RB) in HDF exposed to ionizing γ irradiation (IR, 10 Gy) or treated with ICRF-193 (IC) for indicated times. NT, non-treated cells; SEN, senescent cells. LC, loading control.

F. Violin plots showing nuclear size in non-treated (NT) and HDF treated with ICRF for 48 hr and 12 days. More than 200 cells were analysed in each experiment (n=3). Insert: phase contrast images showing β-galactosidase staining of HDF incubated with ICRF-193 (IC) for two weeks.

G. Representative immunofluorescence images (n=3) showing co-expression of CycD1 and CycA in non-treated (NT) and HDF and ICRF-193 (IC) for 16 hours. Scale bar, 10 μM.

H. Quantification of Cyclin D1 intensity in Cyclin A-positive nuclei in non-treated (NT) and HDF exposed to ICRF-193 (IC) for 8 or 16 hours (% of NT). Cells (>200) were pooled from three independent experiments. Box plot whiskers indicate 10-90% boundary. ***, $p \leq 0.001$, ****, $p \leq 0.0001$**.** In all immunoblots loading controls (LC) were amido-black stained membranes. Red bars indicate RB phosphorylation shift.

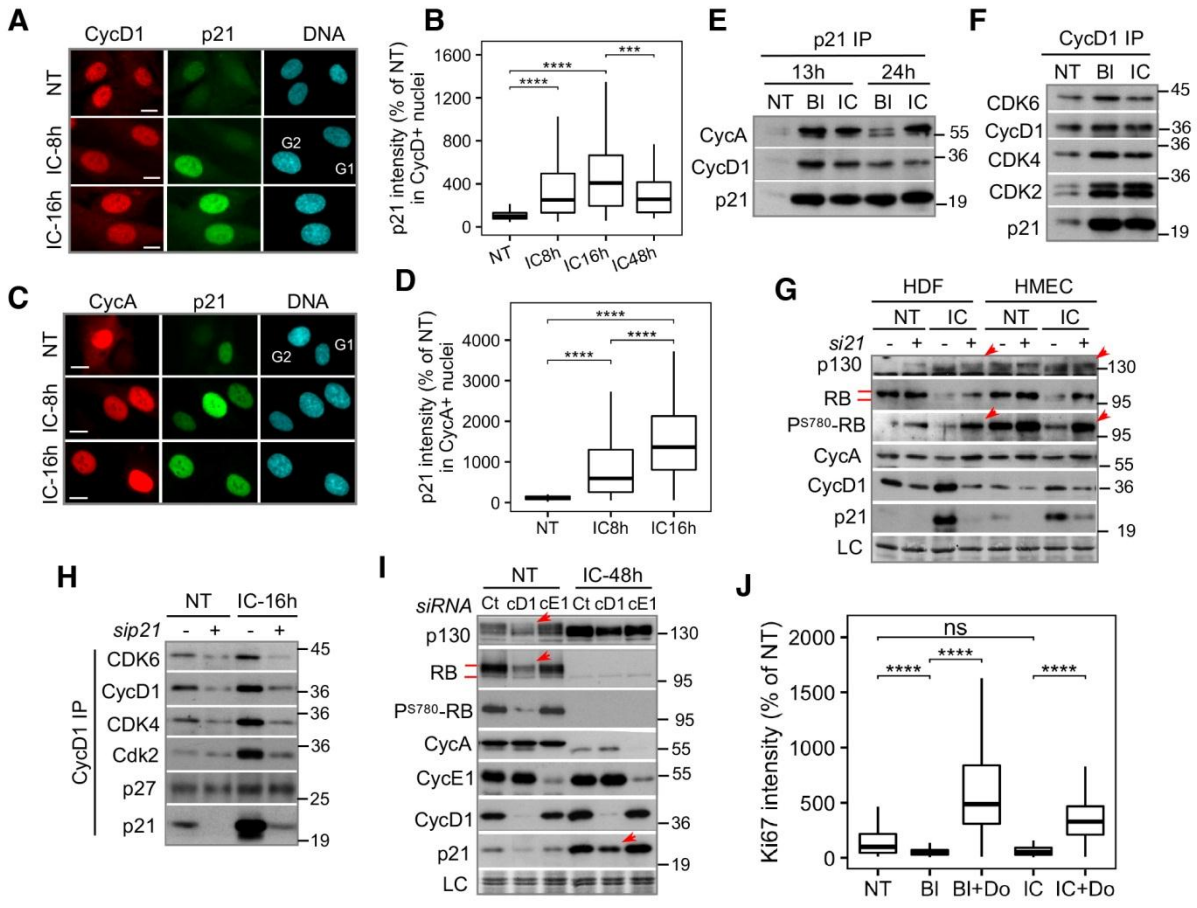

Fig. 2. p21 targets CycD1 to inhibit RB phosphorylation and promote senescence onset after G2 arrest

A. Representative immunofluorescence images (n=3) showing p21 and CycD1 co-localization in HDF incubated with ICRF-193 (IC) for indicated times. Scale bar, 10 μM.

B. Quantification of p21 intensity in CycD1-positive nuclei in non-treated (NT) and HDF incubated with ICRF-193 (IC) for indicated times (% of NT). Cells (>200) were pooled from three independent experiments. Box plot whiskers indicate 10-90 % boundary. ***, $p \leq 0.001$, ****, $p \leq 0.0001$.

C. Representative immunofluorescence images (n=2) showing co-localization of CycA and p21 in HDF incubated with ICRF-193 (IC) for indicated times. Scale bar, 10 μM.

D. Quantification of p21 intensity in CycA-positive nuclei in HDF incubated with ICRF-193 for indicated times. Pooled cells from two independent experiments. n>100. Box plot whiskers indicate 10-90% boundary. **, $p \leq 0.01$, ***, $p \leq 0.001$, ****, $p \leq 0.0001$.

E. Immunoblots showing CycD1 and CycA levels in p21 immunoprecipitates (IP) from extracts of HDF non-treated (NT) or incubated with bleomycin (Bl) or ICRF-193 (IC) for indicated times.

F. Immunoblots showing p21 and CDK levels in CycD1 immunoprecipitates (IP) in lysates from non-treated (NT) and HDF incubated with bleomycin (Bl) or ICRF-193 (IC) for 16 hr.

G. Immunoblots showing effects of p21 depletion (sip21) on CycD1, CycA, p130 and RB levels, and CycD1-specific RB phosphorylation (P^{S780}) in extracts from HDF and HMEC non-treated (NT) or incubated with ICRF-193 (IC) for 16 hr. Red arrows show increased p130 phosphorylation (shift) and P^{S780}-RB after p21 KD (+). LC, loading control.

H. Immunoblots of the indicated proteins in CycD1 immunoprecipitates (IP) from extracts of non-treated (NT) or HDF exposed to ICRF-193 (IC) for 16 hr that were previously depleted (+) or not (-) for p21 (sip21).

I. Immunoblots showing effects of CycD1 (cD1) and CycE1 (cE1) knockdown on p21, CycA, p130 and RB levels and CycD1-specific phosphorylation (P^{S780}-RB) in non-treated (NT) and HDF exposed to ICRF-193 (IC) for 48 hr. Ct, siRNA control. LC, loading control. Red arrows show reduced p130, RB and p21 levels after CycD1 KD.

J. Quantification of Ki67 intensity in T_{121}-expressing fibroblasts exposed to bleomycin (Bl) or ICRF-193 (IC) for 48 hours (% of NT). Doxycycline (Do) was added 12 hr before incubation with genotoxic agents. Pooled cells (>100) from two independent experiments. Box plot whiskers indicate 10-90 % boundary. NT, non-treated cells. Data are representative or mean +/- SEM of at least two independent experiments. ***, $p \leq 0.001$, ****, $p \leq 0.0001$. ns, not significant.

In all immunoblots loading controls (LC) were amido-black stained membranes. Red bars indicate RB phosphorylation shift.

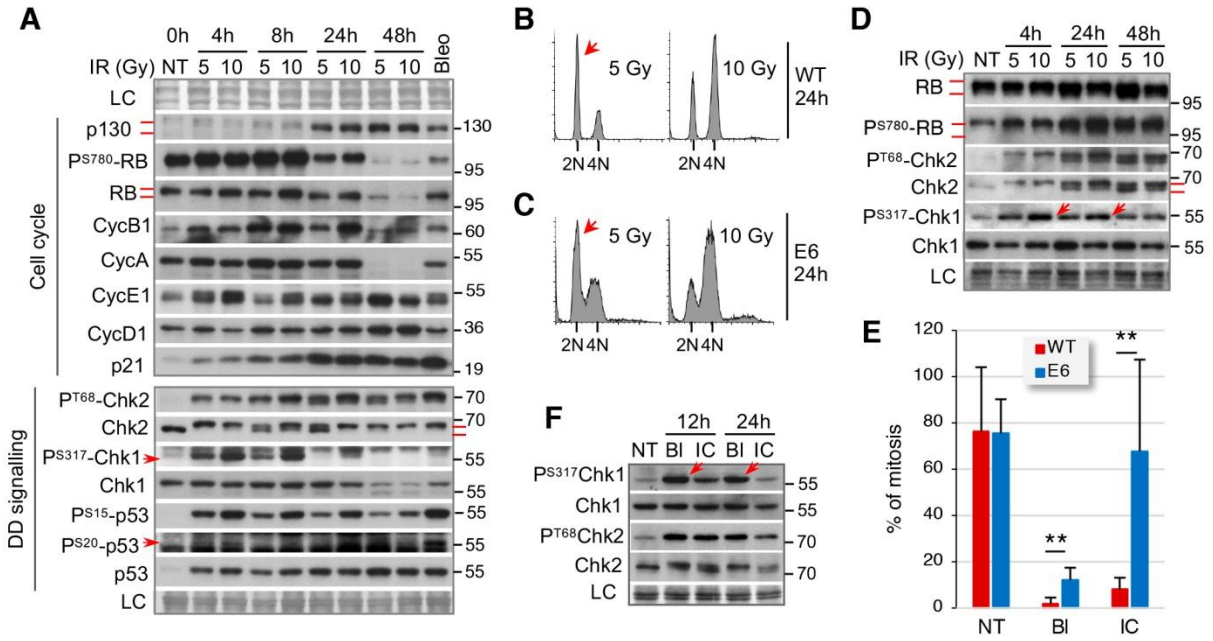

Fig. 3. Chk1 activity drives G2 arrest but its p53-dependent suppression associates with G2 exit

A. Immunoblots of the indicated cell cycle regulators (upper panel) and DNA damage (DD) signalling effectors (lower panel) in HDF that were exposed to ionizing radiation (IR; 5 or 10 Gy) or treated with bleomycin (Bleo-24h) after a release from G0 by contact inhibition (16-24h). FACS is shown in Fig. S1A. NT, non-treated cells (0h time-point); LC, loading control. Red bars indicate p130, RB and Chk2 phosphorylation shifts. Red arrows: P^{S20}-p53 and P^{S317}-Chk1 bands. Red bars: p130, RB and Chk2 phosphorylation shifts.

B. Flow cytometry DNA content profiles of wild-type (WT) and (**C**) HPV16-E6-expressing HDF (E6) collected after 24 hours exposure to ionizing radiation. Red arrows: G1 cells.

D. Immunoblots showing persistent RB and Chk1 phosphorylation and the absence of their down-regulation in HDF-E6 irradiated with 5 or 10 Gy doses. NT, non-treated cells; LC, loading control. Red bars indicate RB and Chk2 phosphorylation shifts. Red arrows indicate stronger P^{S317}-Chk1 signal in 10 Gy.

E. Percent of cells entering mitosis in wild-type (WT) and HPV16-E6-expressing HDF incubated with ICRF-193 (IC) or bleomycin (BL) for 24 hours. Mitosis number was scored from phase contrast images recorded by video-microscopy (mean +/- SD of 3 fields from two separate experiments). **, $p \leq 0.01$.

F. Immunoblots showing phosphorylation of Chk1 (P^{S317}) and Chk2 (P^{T68}) in extracts from HDF expressing HPV16-E6 treated with ICRF193 (IC) or bleomycin (Bl) for indicated times. Red arrows indicate stronger P^{S317}-Chk1 signal in bleomycin-treated cells. NT, non-treated cells; LC, loading control. Complete immunoblot analysis of WT and E6 cells is shown in Fig. S3C.

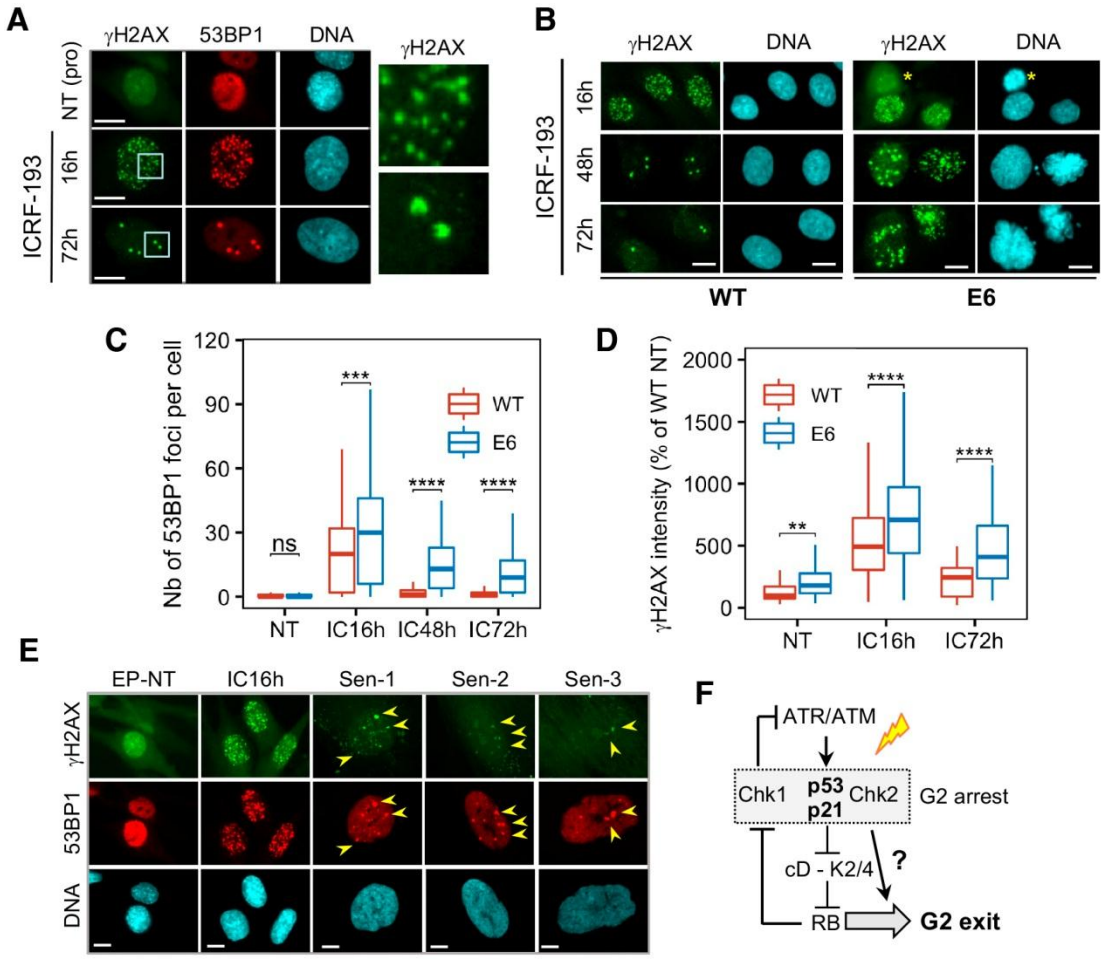

Fig. 4. G2 exit associates with γH2AX downregulation and reduction of DNA damage foci

A. Representative immunofluorescence images (n=3) showing co-localization of γH2AX and 53BP1 foci in non-treated (NT, cell in prophase) and HDF treated with ICRF-193 for indicated times. Scale bar, 10 μM. Right panel shows magnified area to appreciate differences in size/shape of γH2AX foci in cells exposed to ICRF-193 for 16 hr (up) and 72 hr (down).

B. Representative immunofluorescence images (n=2) showing γH2AX foci in WT and E6-expressing HDF treated with ICRF-193 for indicated times. Asterisk (*) denotes cell in prophase. Scale bar, 10 μM.

C. Quantification of 53BP1 foci in WT and E6-expressing HDF exposed to ICRF-193 (IC) for indicated times. NT, non-treated cells. Pooled cells (>200) from three independent experiments. Box plot whiskers indicate 10-90 % boundary. ***,$p \leq 0.001$, ****, $p \leq 0.0001$; ns, not significant.

D. Quantification of nuclear γH2AX foci intensity in WT and E6-expressing HDF exposed to ICRF-193 at indicated timepoints (percent of NT cells). Cells (>100) were pooled from three independent experiments. **, $p \leq 0.01$; ****, $p \leq 0.0001$. Box plot whiskers indicate 10-90 % boundary. NT, non-treated cells.

E. Immunofluorescence images showing co-expression and co-localization of γH2AX and 53BP1 foci in non-treated (NT) early passage HDF (EP-NT), HDF treated with ICRF-193 (IC16h) and in several representative senescent HDF (PD 84). Arrows indicate γH2AX/53BP1 foci in senescent cells. Scale bar, 10 μM.

F. Proposed roles for p53/p21 and CycD1-RB modules in suppressing Ckh1 and ATM/ATR signalling during G2 arrest-G2 exit switch.

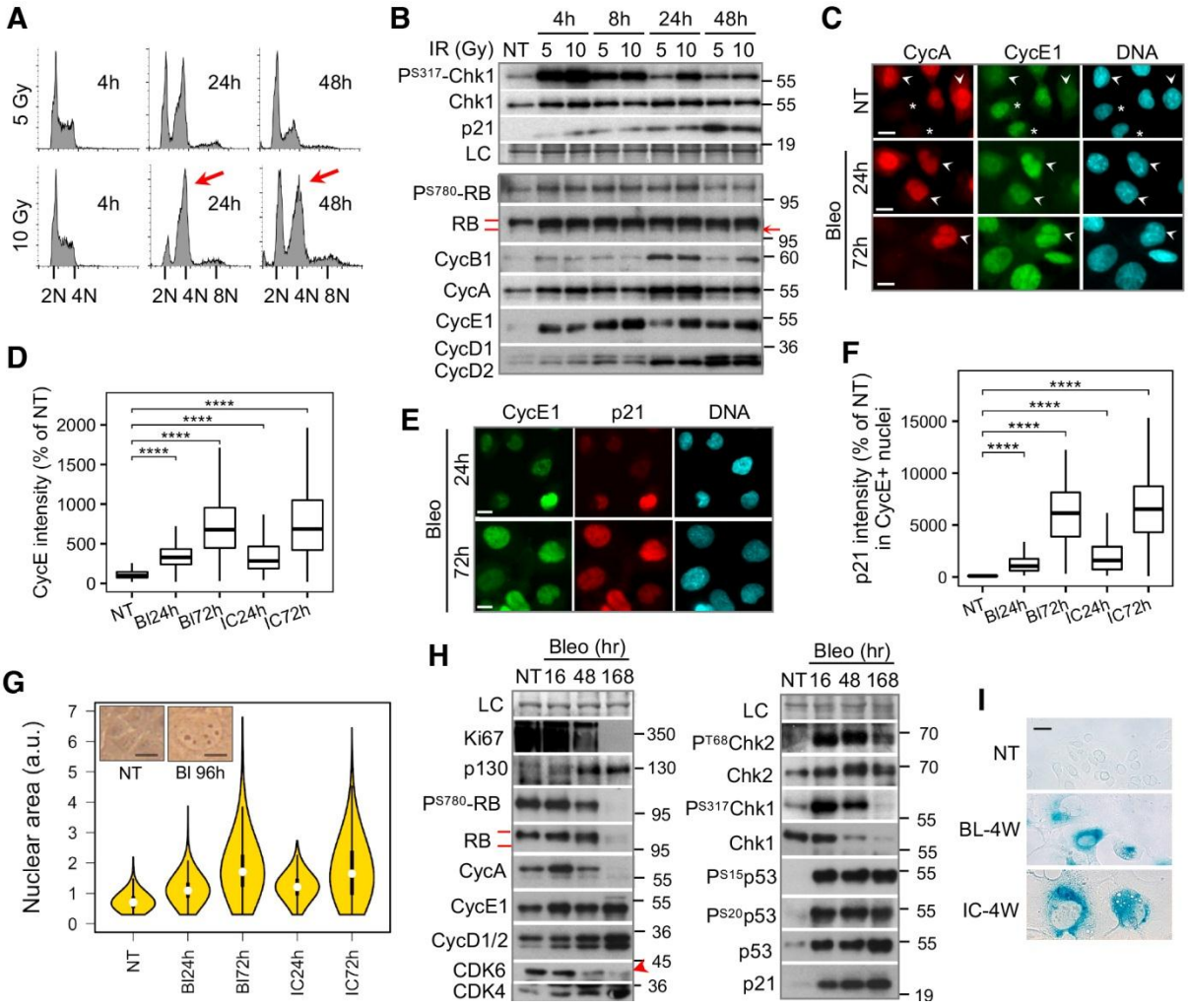

Fig. 5. Sustained Chk1 activation after G2 arrest coincides with altered mitotic bypass and delayed G2 exit in U2OS cells

A. Flow cytometry DNA content profiles of U2OS cells at indicated times after irradiation (5 or 10 Gy). Note more robust G2 arrest in cells irradiated with 10 Gy (red arrows).

B. Immunoblots showing changes in Chk1 phosphorylation, p21 expression (upper panel) and denoted cell cycle regulators (lower panel) in U2OS cells exposed to two doses of ionizing (γ) radiation (IR; 5 or 10 Gy). NT, non-treated cells; LC,

loading control. Red bars: RB phosphorylation shift; red arrow: hypo-phosphorylated RB.

C. Representative immunofluorescence images (n=2) showing CycE1/CycA co-expression in non-treated (NT) and U2OS cells treated with bleomycin (Bleo) for 24 or 72 hours. Asterisk in NT: G1 cells lacking CycA; arrowheads: CycA-positive cells with low (NT) and high (Bleo) CycE1 expression. Scale bar, 10 μM.

D. Quantification of CycE1 intensity in U2OS treated with bleomycin (BL) or ICRF-193 (IC) for 24 or 72 hours (% of NT). Cells (>200) were pooled from two independent experiments. Box plot whiskers indicate 10-90 % boundary. NT, non-treated cells. ****, $p \leq 0.0001$.

E. Representative immunofluorescence images (n=2) showing CycE1/p21 co-expression in U2OS cells treated with bleomycin (Bleo) for indicated times. Scale bar, 10 μM.

F. Quantification of p21 intensity in CycE1-expressing U2OS cells treated with bleomycin for indicated times (% of NT). Cells (>200) were pooled from two independent experiments. Box plot whiskers indicate 10-90 % boundary. ***, $p \leq 0.0001$. NT, non-treated cells.

G. Violin plots showing nuclear size in non-treated (NT) and U2OS exposed for 24 and 72 hours to bleomycin (Bleo) or ICRF-193 (ICRF). More than 500 cells were analysed in each experiment (n=2). Inserts are micrographs showing NT and cells exposed for 96 hr to bleomycin. Scale bar, 10 μM.

H. Immunoblots showing effects of prolonged incubation with bleomycin (Bleo) on indicated cell cycle regulators (left panel) and DNA damage signalling effectors (right panel) in U2OS cells. NT, non-treated cells; LC, loading control. Arrowhead (left panel) shows CDK6 downregulation.

I. Phase contrast images showing β-galactosidase staining of U2OS cells exposed to bleomycin (Bl) or ICRF-193 (IC) for 4 weeks. Scale bar, 10 μM.

In all immunoblots loading controls (LC) are amido-black stained membranes. Red bars: RB phosphorylation shift.

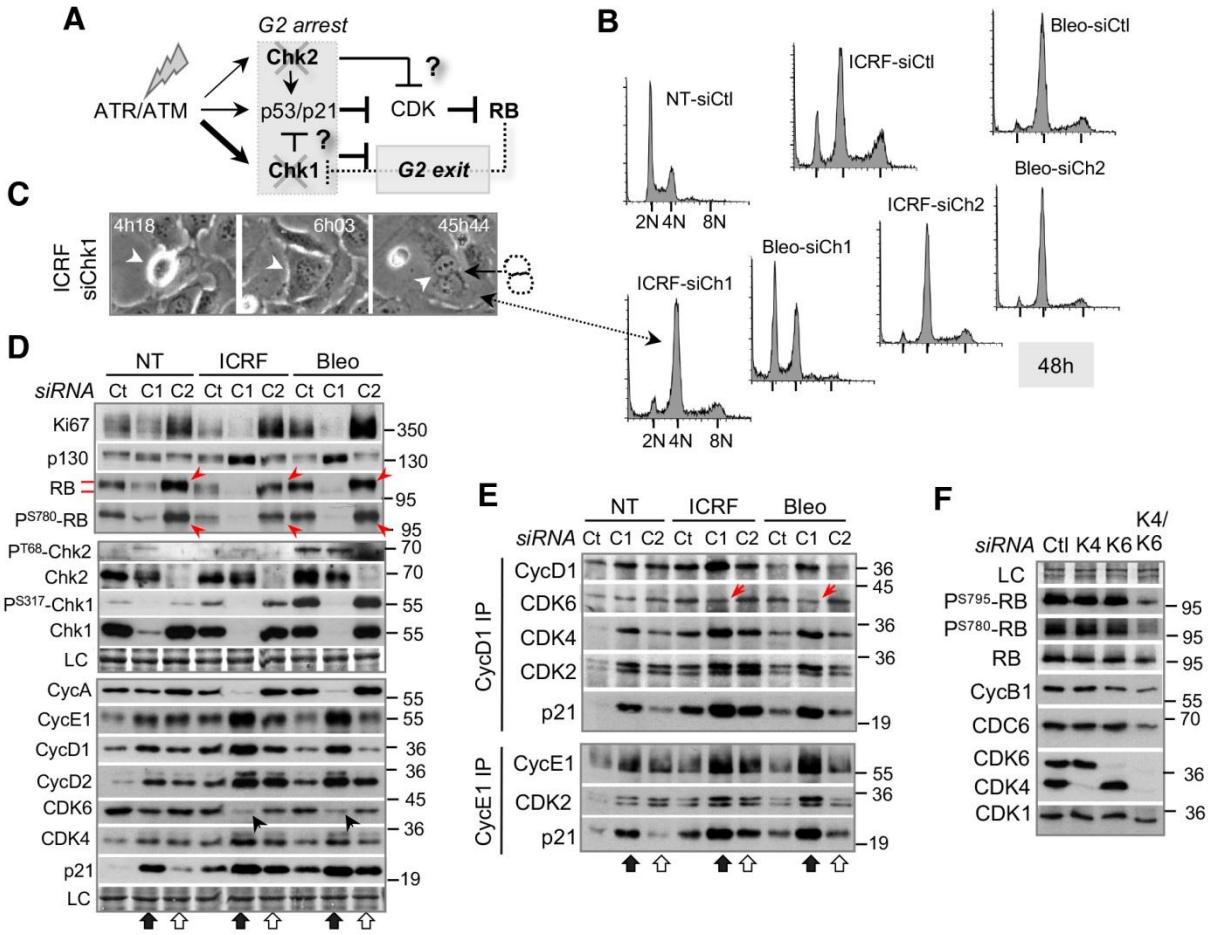

Fig. 6. Chk1, but not Chk2, depletion promotes DNA damage-induced cell cycle exit by inhibiting RB kinases

A. Model: Expected effects of Chk1 and Chk2 knockdown on RB pathway and DNA damage-induced G2 arrest/exit switch.

B. Flow cytometry DNA content profiles of non-treated (NT-siCtl) and siCtl, siChk1 and siChk2 U2OS cells treated with bleomycin (Bleo) and ICRF-193 (ICRF) for 48 hr. See Fig.S6A for NT-siChk1 and NT-siChk2.

C. Phase contrast images from video-microscopy sequences showing binuclear daughter cell after mitosis and cytokinesis failure (arrowheads) in U2OS Chk1 KD cells treated with ICRF-193 (ICRF). Time after the addition of the drug is indicated.

D. Immunoblots showing effects of Chk1 (C1-black arrow) and Ckh2 (C2-white arrow) knockdown on Ki67 levels, RB phosphorylation and expression of the indicated cell cycle regulators in non-treated (NT) and U2OS cells treated with ICRF-193 (ICRF) or bleomycin (Bleo) for 48 hr. Ct, control siRNA. LC, loading control. See Fig. S6B for 16 hr time-point. Red bars indicate RB phosphorylation shift. Red arrows indicate increased RB phosphorylation in Chk2 depleted samples. Black arrows indicate reduction of CDK6 in Chk1 depleted samples.

E. Immunoblot analysis of Cyclin D1 and Cyclin E1 immunoprecipitates (IP) showing effects of Chk1 (C1-black arrow) and Chk2 (C2-white arrow) knockdown on cyclin-CDK-p21 complexes in U2OS exposed to ICRF-193 (ICRF) and bleomycin (Bleo) for 48 hr. Red arrows: reduction of CDK6 in CycD1 complexes.

F. Immunoblots showing effects of CDK4 (K4), CDK6 (K6) or double CDK4 / CDK6 (K4/K6) knockdown on Cyclin D1-specific RB phosphorylation (P^{S795}, P^{S780}) in U2OS cells. Loading controls (LC) are amido-black stained membranes.

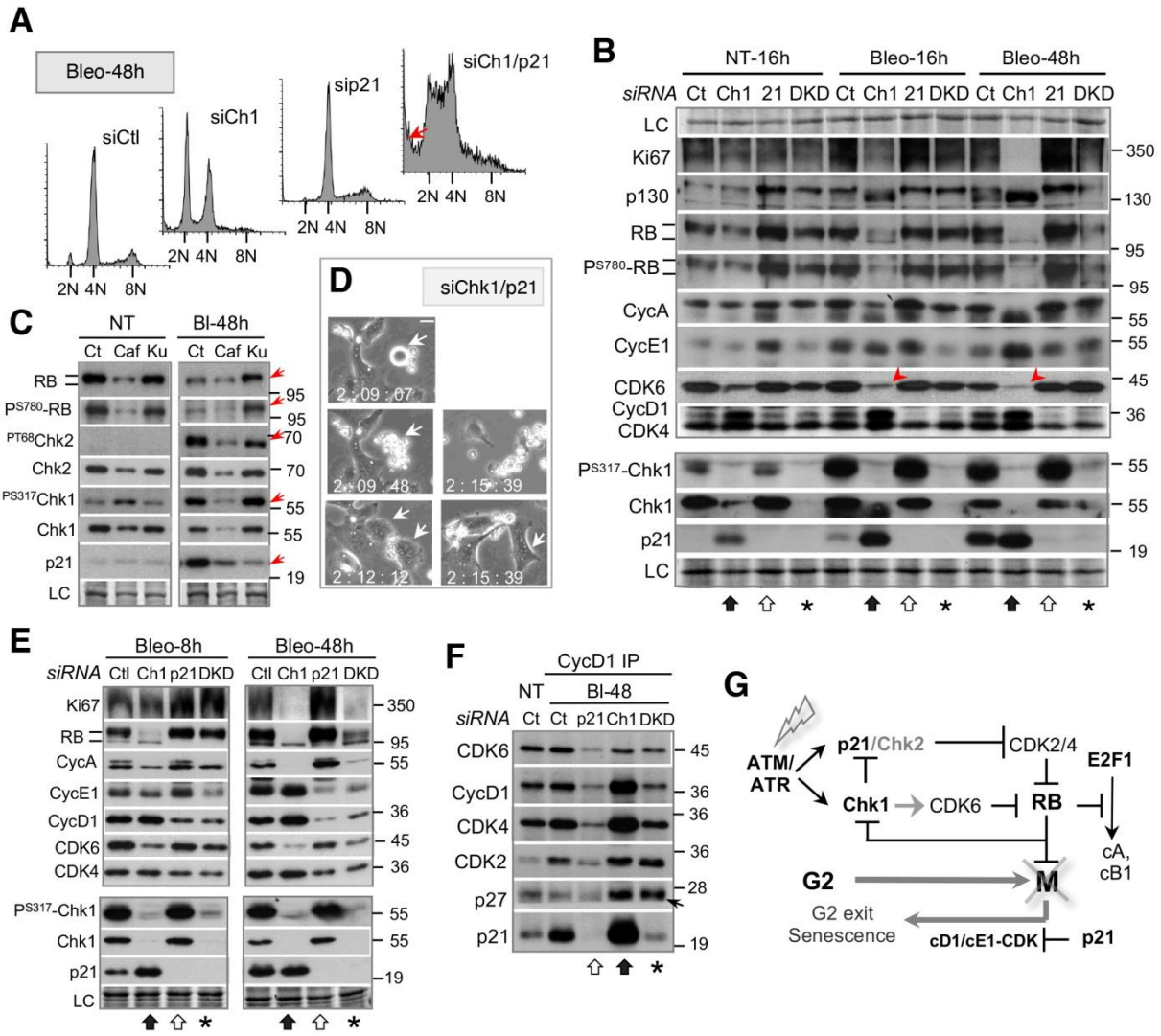

Fig. 7. Chk1 knockdown in cancer cells accelerates cell cycle exit by inducing p21 and downregulating CDK6

A. Flow cytometry DNA content profiles of control (siCtl) and U2OS cells depleted for Chk1 (siCh1), p21 (sip21) or both (siCh1/21) proteins treated with bleomycin (Bleo) for 48 hours. Red arrow indicates sub-G1 population representing dead cells. See Fig. S7A for FACS results showing effects of respective knockdowns on non-treated and U2OS treated with bleomycin (Bleo) for 16 hr.

B. Immunoblots showing effects of Chk1 (Ch1-black arrow), p21 (21, white arrow) or double p21/Chk1 (DKD-asterisk) knockdown on Ki67 and indicated cell cycle regulators (upper panel) and DNA damage signalling effectors (lower panel) in non-treated (Ctl) and U2OS cells treated with bleomycin (Bleo) for 16 and 48 hours. LC, loading control. Red arrowheads indicate downregulated CDK6.

C. Immunoblots showing effects (red arrows) of caffeine (Caf) and ATM inhibitor KU-55933 (Ku) on RB protein and phosphorylation (P^{S780}) levels, P^{T68}-Chk2, P^{S317}-Chk1 and p21 levels in non-treated (NT) and U2OS cells treated with bleomycin for 48 hr (arrows). LC, loading control.

D. Representative phase contrast images from a video-microscopy sequence showing fragmented nuclei after mitotic catastrophe in bleomycin-treated double Ckh1/p21 KD cells. Time (days, hours, minutes) after drug adding is indicated. Arrows show mitotic cell and resulting daughter cells. Most right-hand image (upper panel) shows cell debris from the same sequence. Complete field is shown in Fig. S7D. Scale bar, 10 μM.

E. Immunoblots showing effects of Chk1 (Ch1-black arrow), p21 (white arrow) or double p21/Chk1 (DKD- black asterisk) knockdown on Ki67 and the indicated cell cycle regulators in HCT-116 cells treated with bleomycin (Bleo) for 8 and 48 hours. LC, loading control.

F. Immunoblots of CycD1 immunoprecipitates (IP) showing effects of Chk1 (Ch1, black arrow), p21 (white arrow) or double p21/Chk1 (DKD-asterisk) knockdown on cyclin-CDK-CKI complexes in HCT-116 cells exposed to bleomycin (Bl) for 48 hr.

In all blots black bars indicate RB phosphorylation shift and loading controls (LC) are amido-black stained membranes.

G. Proposed roles for Chk1, Chk2 and p21-CycD-RB axis in DNA damage-induced senescence onset after permanent G2 arrest (G2 exit).

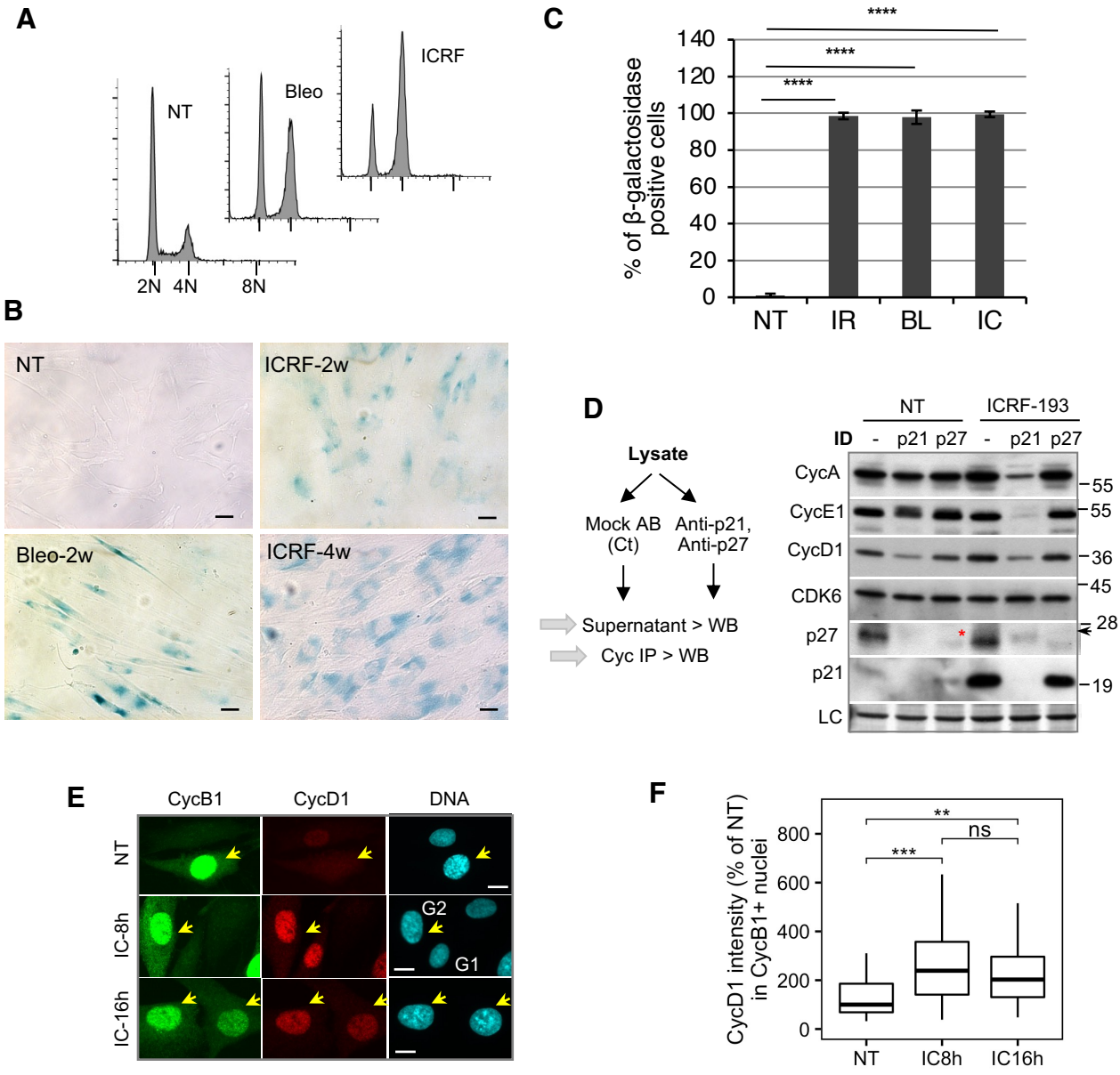

Fig. S1. DNA damage-induced cell cycle arrest in G2 leads to cell cycle exit and senescence

A. Flow cytometry DNA content profiles of the asynchronously growing non-treated (NT) and HDF exposed to bleomycin (Bleo) or ICRF-193 (ICRF) for 48 hours.
B. Representative phase-contrast images showing β-galactosidase staining of non-treated (NT) and HDF exposed to ICRF-193 (ICRF) for 2 and 4 weeks (n=2). NT, non treated cells. Scale bar, 5 μM.
C. Quantification of β-galactosidase staining in HDF exposed to γ irradiation (IR, 10Gy), ICRF-193 (IC) or bleomycin (BL) for two weeks. NT, non treated cells. Data are mean +/- s.d. of at two independent experiments.
p values were calculated with two-sided Student's *t* test; ****, $p \leq 0.0001$.
D. p21/p27 immunodepletion (ID) experiment. Left: experimental design. Right: Immunoblots showing CycE1, CycA, CycD1 and CDK6 levels before (mock-treated: Ct (-)) or after immunodepletion (ID) of p21 or p27 from the lysates prepared from NT (non treated) and HDF exposed to ICRF-193 (16h). LC, loading control is amido-black stained membrane. Arrow indicates position of p27 band. Red asterisk indicates immunoblot artefact.
E. Representative immunofluorescence images (n=2) showing co-localization of CycB1 and CycD1 in non-treated (NT) and HDF exposed to ICRF-193 (IC) for 8h and 16h. Scale bar, 10 μM. Arrows points at cells expressing nuclear CycB1.
F. Quantification of CycD1 intensity in CycB1-positive HDF exposed to ICRF-193 (IC) for indicated times. Cells (n>100) were pooled from two independent experiments. Box plot whiskers indicate 10-90% boundary.

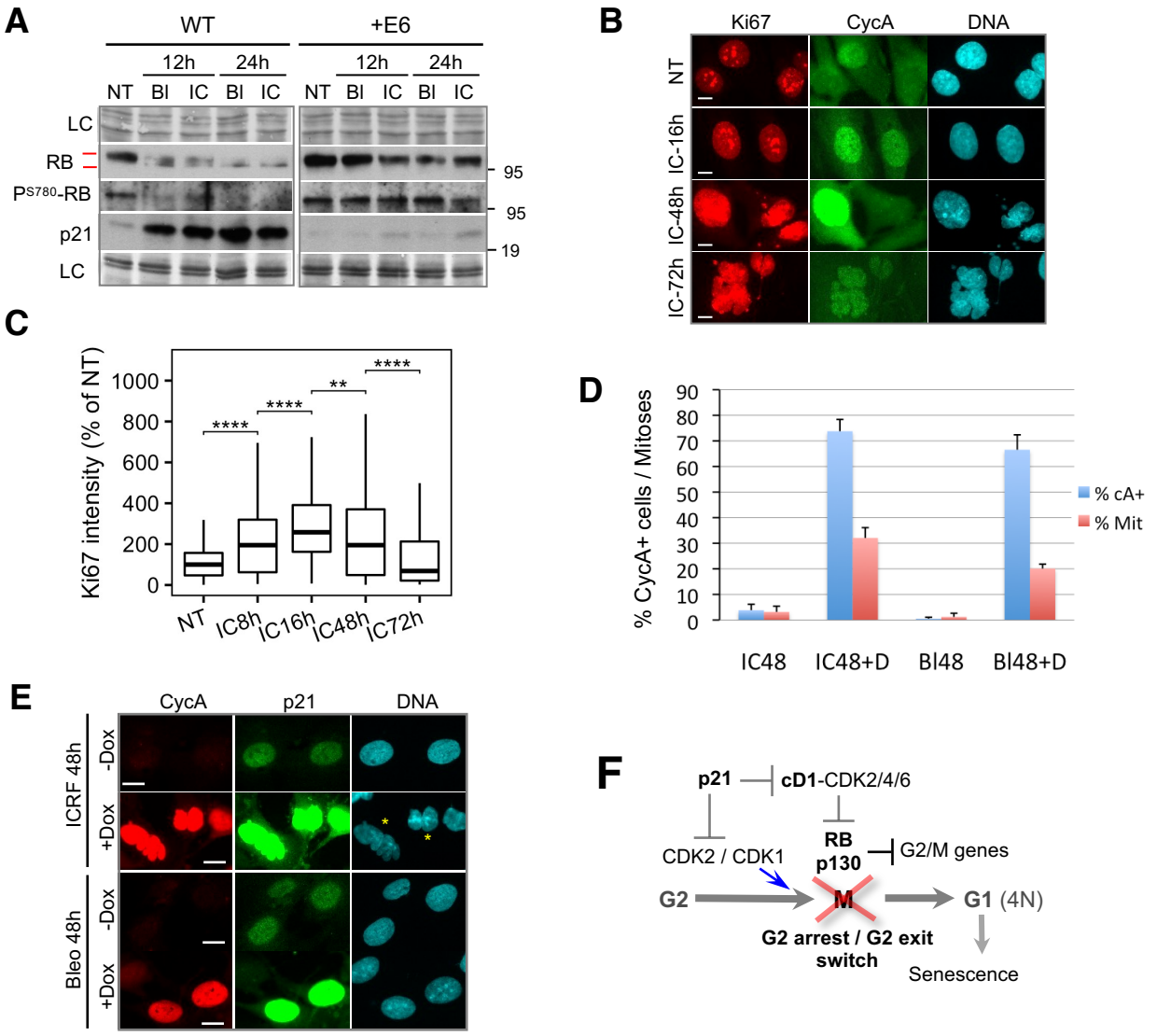

Fig. S2. HPV-E6-mediated p53 degradation and inactivation of pocket proteins by the T_{121} mutant of SV40 oncogene compromises G2 exit in human fibroblasts

A. Immunoblots showing persistent CycD1-specific RB phosphorylation (P^{S780}) in p21-deficient HPV16-E6 expressing HDF (E6) exposed to bleomycin (BI) or ICRF-193 (IC) for 12 and 24h. Loading controls (LC) were amido-black stained membranes. Red bars indicate RB phosphorylation shift.
B. Representative immunofluorescence images (n=2) showing expression of Ki67 and CycA in HDF-E6 exposed to ICRF-193 (IC) for indicated times. Scale bar, 10 μM.
C. Quantification of Ki67 intensity in the nuclei of HDF-E6 exposed to ICRF-193 (IC) for indicated times. Cells (n>100) were pooled from two independent experiments. Box plot whiskers indicate 10-90% boundary. p values were calculated with two-sided Student's *t* test; **, $p \leq 0.01$; ****, $p \leq 0.0001$. NT, non-treated cells.
D. CycA positive (cA+) cells and mitotic cells (Mit, DAPI) were scored from immunofluorescence images taken at the indicated time points after the drug addition. T_{121}-expressing fibroblasts were exposed to bleomycin (BI) or ICRF-193 (IC) for 48 hours. Doxycycline (D) was added 12h prior to drug treatment (+). More than 100 cells were analyzed in each experiment. Data are mean +/- SEM of two independent experiments.
E. Representative immunofluorescence images (n=2) showing co-expression of CycA and p21 in the presence of ICRF-193 (ICRF) and bleomycin (Bleo) in T_{121}-expressing fibroblasts. Asterisks denote binuclear cells generated by unsuccessful cytokinesis after mitosis. Experimental conditions were as above. Dox, doxycycline. Scale bar, 10 μM.
F. Model proposing the role of p21-mediated CycD1-CDK2/4 inhibition in the G2 arrest / G2 exit switch preceding senescence.

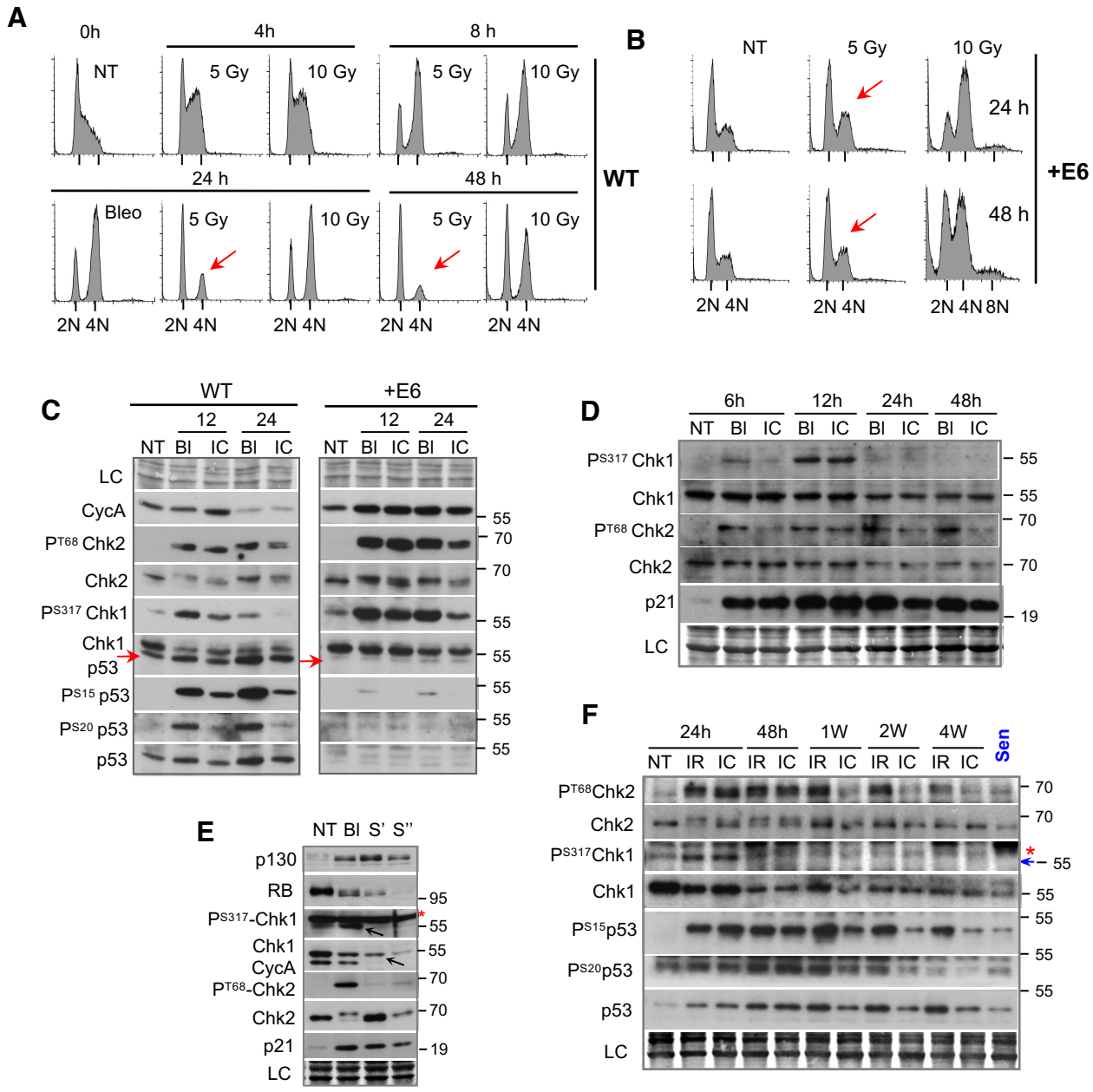

Fig. S3. G2 exit correlates with p53-dependent downregulation of Chk1 signaling

A. Flow cytometry DNA content of wild-type (WT) HDF at indicated times after irradiation. Cells were irradiated (5 or 10 Gy) or exposed to bleomycin (Bleo, 24) 16 hours after release from quiescence by contact inhibition. Arrows indicate lower amount of cells arrested in G2. NT, non-treated cells (0h time-point);
B. Flow cytometry DNA of HDF expressing HPV16-E6 (+E6) 24 and 48 hours after irradiation. Asynchronous cells were exposed to 5 or 10 Gy. NT, non-treated control.
C. Immunoblots showing phosphorylation of Chk1 (P^{S317}), Chk2 (P^{T68}) and p53 (P^{S15}, P^{S20}) as well as p21 induction in wild-type (WT) and HDF expressing HPV16-E6 (+E6) exposed to ICRF193 (IC) or bleomycin (BI) for indicated times. NT, non-treated cells; LC, loading control. Red arrows show p53 band.
D. Immunoblots showing down-regulation of Chk1 phosphorylation (P^{S317}-Chk1) and sustained Chk2 (P^{T68}-Chk2) phosphorylation in HDF exposed to ICRF-193 (IC) or bleomycin (BI) at indicated times. NT, non treated cells; LC, loading control.
E. Immunoblots of the indicated cell cycle regulators and DNA damage signalling proteins in extracts of early passage (population doubling (PD) 30), non-treated (NT) or exposed to bleomycin (BI-12h), and senescent HDF (S' - PD 74; S'' - PD 84). Arrows: P^{S317}-Chk1 and Chk1 bands; Red asterisk: nonspecific band. LC, loading control.
F. Immunoblots showing down-regulation of Chk1 phosphorylation (P^{S317}-Chk1) and sustained Chk2 (P^{T68}-Chk2) phosphorylation in HDF upon γ irradiation (IR, 10 Gy) or treatment with ICRF-193 (IC) for indicated times. NT, non-treated cells; Sen, senescent cells. LC, loading control. Arrow: P^{S317}-Chk1 band; Red asterisk: nonspecific band.
In all immunoblots loading controls (LC) were amido-black stained membranes.

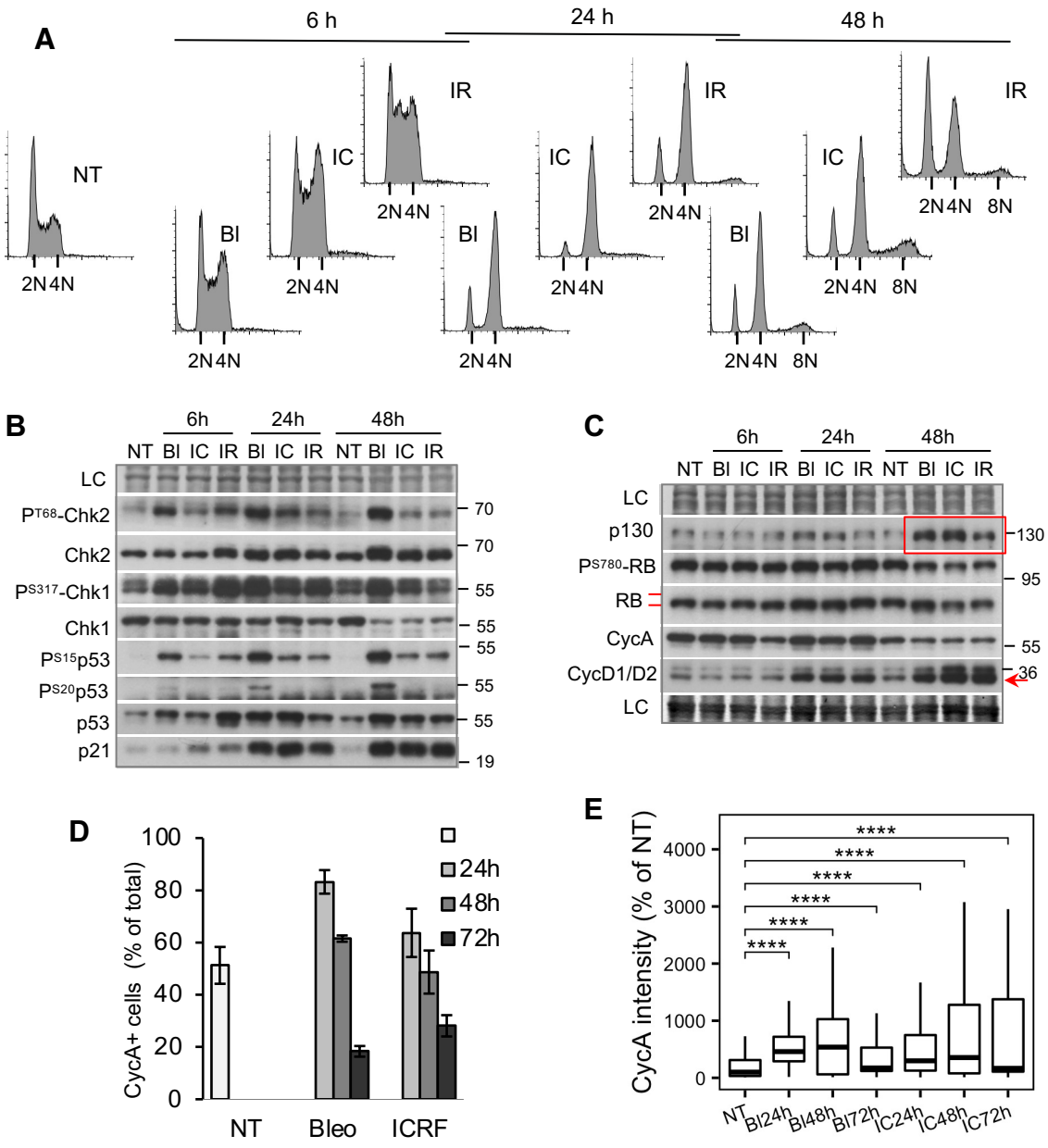

Fig. S4. Sustained Chk1 activity in G2-arrested U2OS cells coincides with altered mitotic bypass and delayed G2 exit

A. Flow cytometry DNA content profiles of non treated (NT) and U2OS cells exposed to bleomycin (BI), ICRF-193 (IC) or irradiation (IR, 10 Gy) for indicated times.
B. Immunoblot analysis showing changes in DNA damage response effectors in U2OS cells after γ-radiation (IR, 10 Gy) or exposure to bleomycin (BI) or ICRF-193 (IC) for indicated times. NT, non-treated cells. LC, loading control.
C. Immunoblot analysis showing changes in cell cycle control regulators. Red bars indicate RB phosphorylation shift, red arrow shows CycD2 band and red rectangle shows accumulation of hypo-phosphorylated p130. In all immunoblots loading controls (LC) are amido-black stained membranes.
D. Quantification of CycA positive cells (% of total cell numbers) in immunofluorescence images taken at the indicated time-points after exposure to bleomycin (Bleo) or ICRF-193 (ICRF). Data are mean +/- SEM of three independent experiments. n>100.
E. Quantification of nuclear CycA intensity (immunofluorescence) in U2OS cells exposed to bleomycin (BL) or ICRF-193 (IC) for indicated times. Cells (n>100) were pooled from two independent experiments. Box plot whiskers indicate 10-90% boundary. NT, non-treated cells. *p* values were calculated with two-sided Student's *t* test; ****, p ≤ 0.0001.

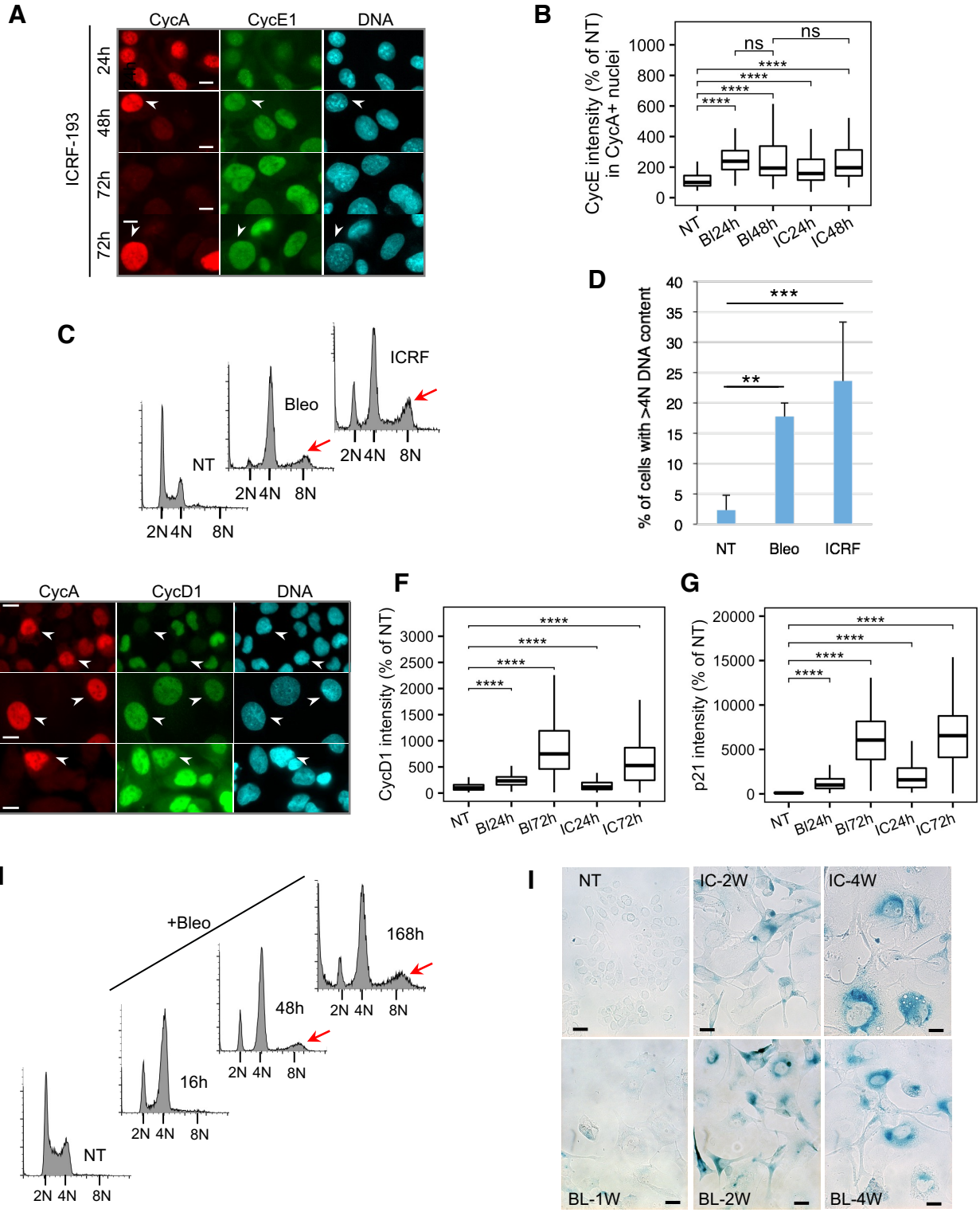

Fig. S5. DNA damage-induced G2 arrest in U2OS leads to aberrant upregulation of G1 cyclins coinciding with p21 induction, genome re-duplication and delayed senescence onset in G2.

A. Representative immunofluorescence images (n=2) showing CycA/CycE1 co-expression in U2OS cells exposed to ICRF-193 for indicated times. Arrowheads show CycA-positive cells with high CycE1 expression. Scale bar, 10 μM.
B. Quantification of CycE1 intensity in CycA-positive nuclei in non-treated (NT) or U2OS cells exposed to bleomycin (Bl) or ICRF-193 (IC) for 24 or 48 hours. Cells (n>200) were pooled from two independent experiments. Box plot whiskers indicate 10-90% boundary.
C. Flow cytometry analysis of DNA content of non-treated (NT) and U2OS cells exposed to bleomycin (Bleo) and ICRF-193 (ICRF) for 48 hrs. Red arrows indicate 8N population as a result of DNA re-replication in G2 arrested cells.
D. Percent of cells with >4N DNA content in non- treated (NT) and U2OS cells exposed to bleomycin and ICRF-193 (ICRF) for 48 hrs. Data are mean +/- s.d. of five independent experiments. *p* values were calculated with two-sided Student's *t* test; **, $p \leq 0.01$; ***, $p \leq 0.001$.
E. Representative immunofluorescence images (n=2) showing CycA/CycD1 co-expression in U2OS cells exposed to bleomycin (Bleo) for indicated times. Arrowheads show CycA-positive cells with high CycD1 expression. Bar, 10 μM.
F. Quantification of nuclear CycD1 intensity in U2OS cells exposed to ICRF-193 or bleomycin for indicated times. Cells (n>100) were pooled from two independent experiments. Box plot whiskers indicate 10-90% boundary. NT, non-treated cells.
G. Quantification of nuclear p21 intensity in U2OS cells exposed to bleomycin (Bl) or ICRF-193 (IC) for indicated times. Cells (n>100) were pooled from two independent experiments. Box plot whiskers indicate 10-90% boundary. NT, non-treated cells.
H. Flow cytometry DNA content profiles of non-treated (NT) and U2OS cells treated with bleomycin (Bleo) for 16, 48 and 168 hours. Red arrows indicate the cells that underwent re-replication after prolonged DNA damage (8N).
I. Representative phase-contrast images showing β-galactosidase staining of non treated (NT) and U2OS cells exposed to ICRF-193 (ICRF) or bleomycin (Bleo) for 1 week (W), 2 weeks and 4 weeks. Scale bar, 10 μM.

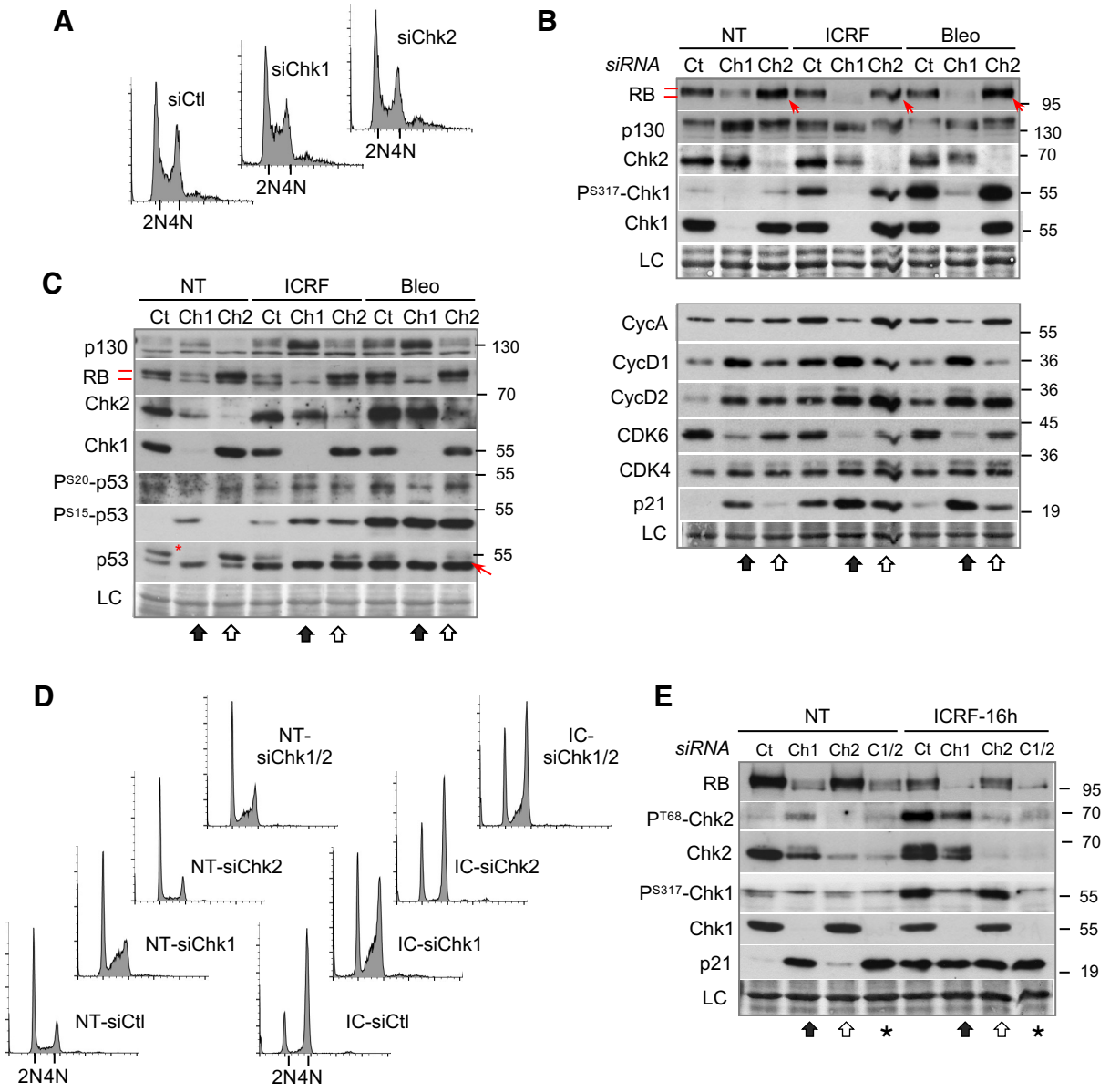

Fig. S6. Chk1 knockdown accelerates whereas Chk2 knockdown delays DNA damage-induced cell cycle exit.

A. Flow cytometry DNA content profiles of asynchronously growing U2OS cells 24 hours after siRNA-mediated Chk1 (siChk1) or Chk2 (siChk2) knockdown.
B. Immunoblots showing effects of Chk1 (Ch1, black arrow) and Chk2 (Ch2, white arrow) knockdown on RB and p130 phosphorylation (upper panel) and expression of cell cycle regulators (lower panel) in non-treated (NT) and U2OS cells exposed to ICRF-193 (ICRF) or bleomycin (Bleo) for 16h. Red arrows: increased RB levels after siChk2. LC, loading control.
C. Immunoblots showing effects of Chk1 (Ch1, black arrow) and Chk2 (Ch2, white arrow) knockdown on p53 phosphorylation (P^{S20}, P^{S15}) in non-treated (NT) and U2OS cells exposed to ICRF-193 (ICRF) or bleomycin (Bleo) for 48h. Red arrow: p53 band. Red asterisk: Chk1 band. LC, loading control.
D. Flow cytometry DNA content profiles of asynchronously growing non-treated (NT) and HDF exposed to ICRF-193 (IC, 16h) 24 hours after siRNA-mediated Chk1 (siChk1), Chk2 (siChk2) or double Chk1/Chk2 (siChk1/2) knockdown.
E. Immunoblots showing effects of Chk1 KD (Ch1, black arrow), Chk2 (Ch2, white arrow) and double Chk1/Chk2 (C1/2, asterisk) knockdown on RB phosphorylation and p21 induction in non-treated (NT) and HDF treated with ICRF-193 (ICRF) for 16h. LC, loading control.
In all immunoblots loading controls (LC) are amido-black stained membranes.

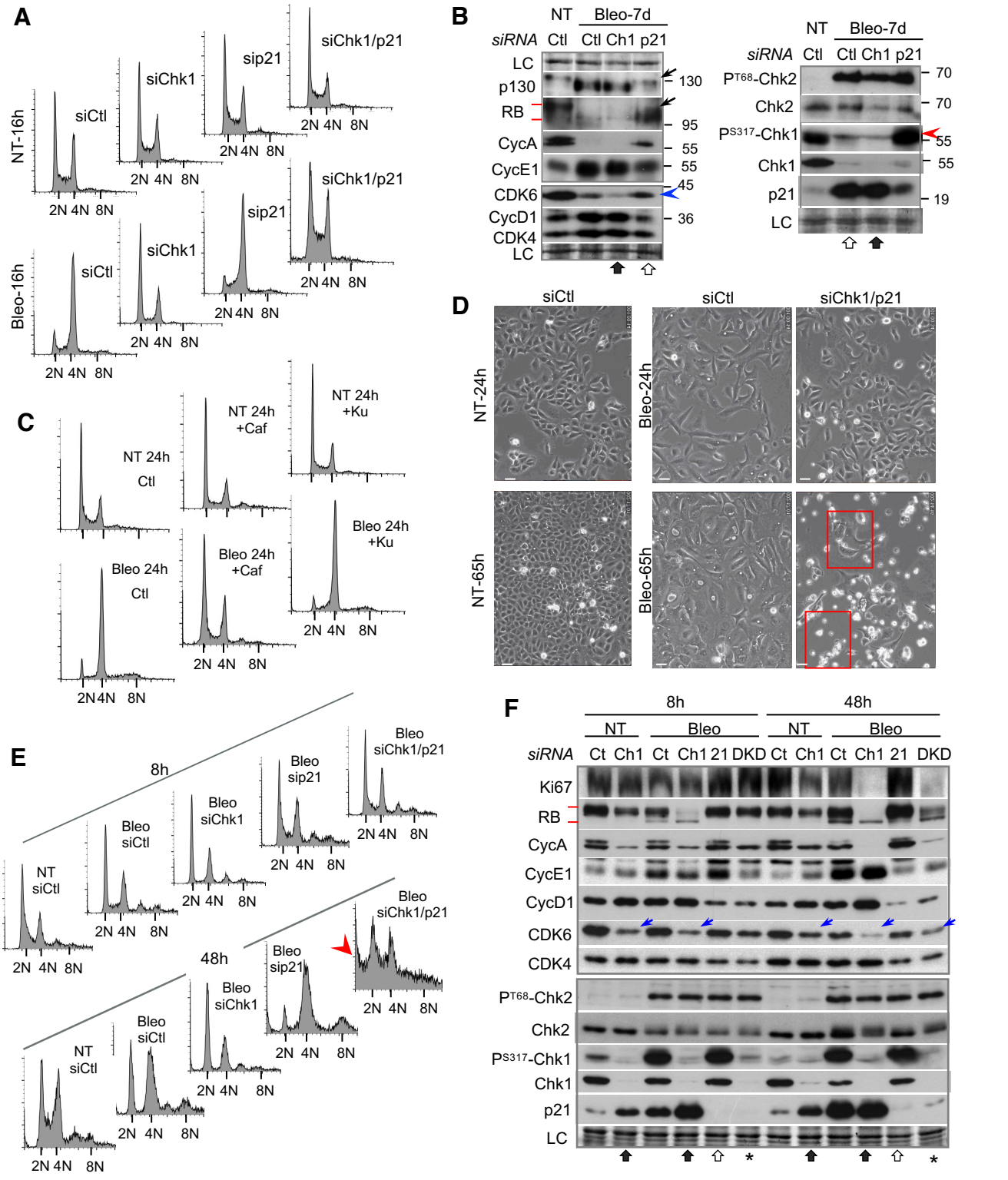

Fig. S7. Chk1 knockdown in cancer cells accelerates cell cycle exit by inducing p21 and downregulating CDK6

A. Flow cytometry DNA content profiles of non-treated control (siCtl) and bleomycin-treated U2OS cells depleted for Chk1 (siChk1), p21 (sip21) or both proteins (siChk1/p21) after 16 hours.
B. Immunoblots showing effects of Chk1 (Ch1-black arrow) or p21 knockdown (white arrow) on pocket protein phosphorylation and expression of different cell cycle regulators in non-treated (NT) and U2OS cells exposed to bleomycin (Bleo) for 7 days. Black arrows: elevated p130 and pRb hyper-phosphorylation after p21 depletion. Red arrowhead: strong PS317-Chk1 signal in the absence of p21. Blue arrowhead indicates low Cdk6 levels. Red bars indicate RB phosphorylation shift. LC, loading control.
C. Flow cytometry DNA content profiles of non-treated (NT) and U2OS cells exposed to bleomycin for 24h. Caffeine (Caf) and KU-55933 (Ku) were added one hour before treatment.
D. Representative phase contrast images from a single video-microscopy sequence showing bleomycin-treated control (siCtl) and double Chk1/p21 knock down (siChk1/p21) U2OS cells at different times after exposure to the drug. Red rectangles show the inserts presented in Figure 7C. Scale bar, 20 μM.
E. Flow cytometry DNA content profiles of non-treated control (siCtl) and bleomycin-treated HCT-116 cells depleted for Chk1 (siChk1), p21 (sip21) or both (siChk1/p21) proteins after 8 and 48 hours. Red arrow indicates the presence of sub-G1 population associated with dying cells after 48h in bleomycin-treated siChk1/p21 cells.
F. Immunoblots showing effects of Chk1 (Ch1-black arrow), p21(white arrow) or double p21/Chk1 (DKD-asterisk) knockdown on Ki67,RB phosphorylation, expression of different cell cycle regulators and DNA damage response (P^{T68}-Chk2, P^{S317}-Chk1, p21) in non-treated (NT) and HCT-116 cells exposed to bleomycin (Bleo) for 8 and 48 hours. Blue arrows indicate low Cdk6 levels after Chk1 depletion. LC, loading control.
In all immunoblots loading controls (LC) are amido-black stained membranes. Red bars indicate RB phosphorylation shift.

Table S1. List of antibodies used

Click here to download Table S1

Figure 1A

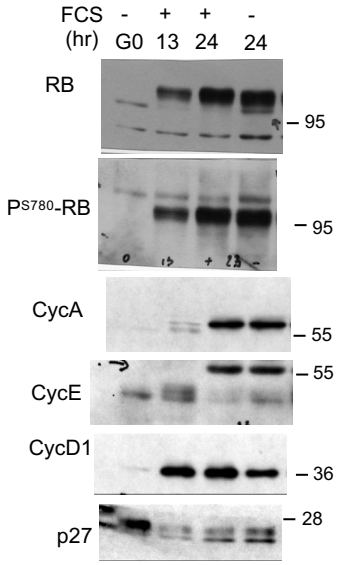

Figure 1B

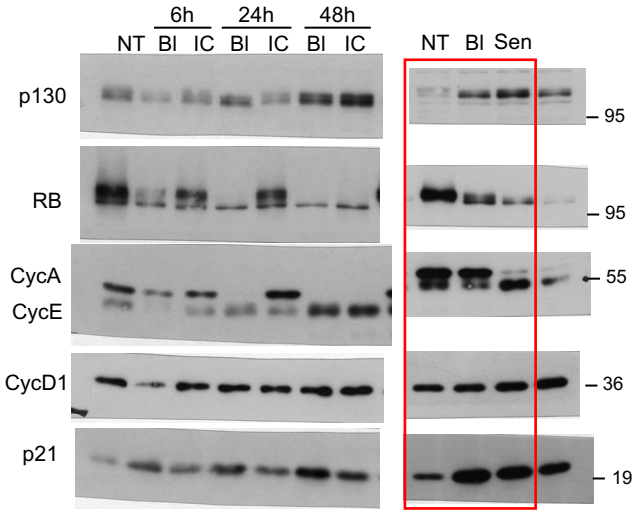

Figure 1E

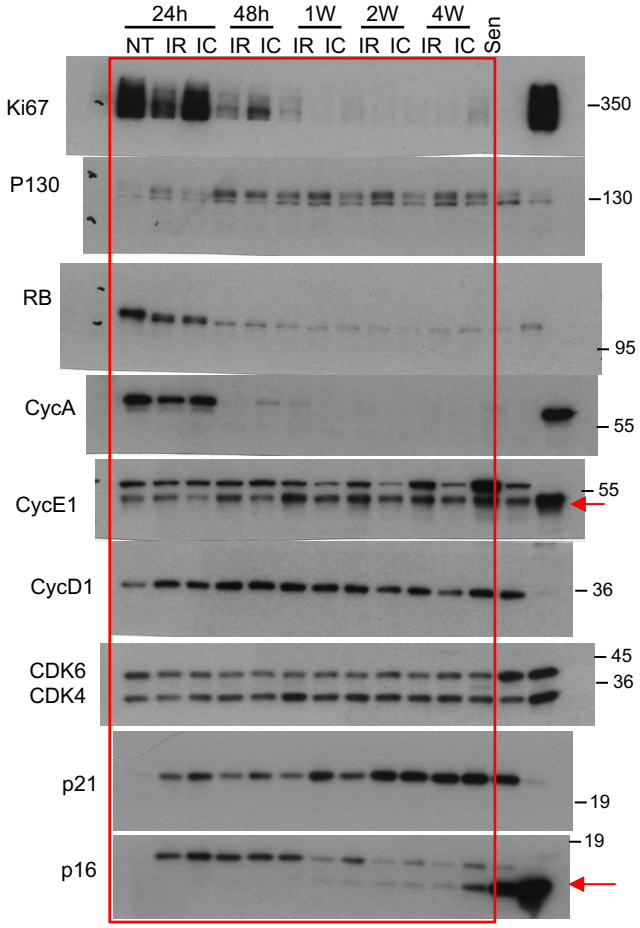

Figure 1S

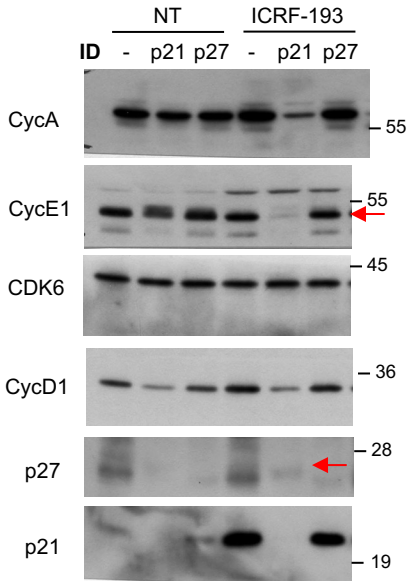

Figure 2E

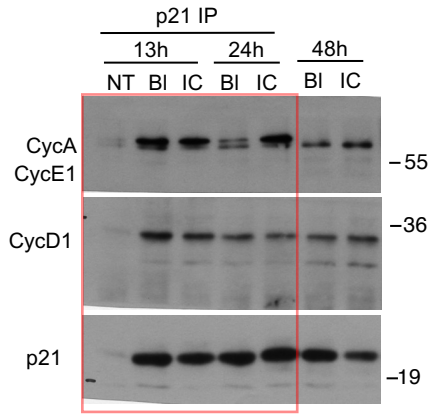

Figure 2F

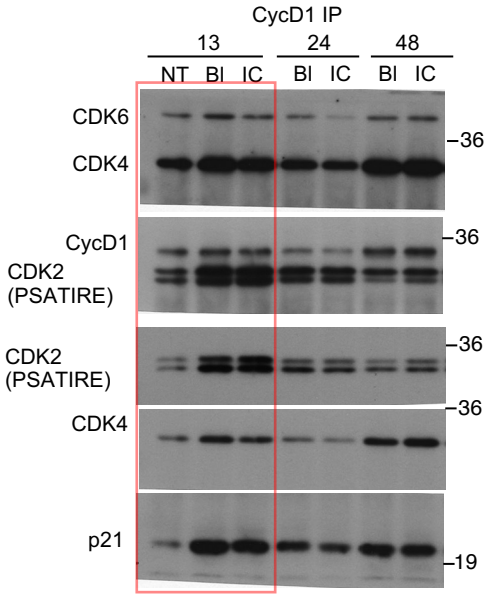

Figure 2G

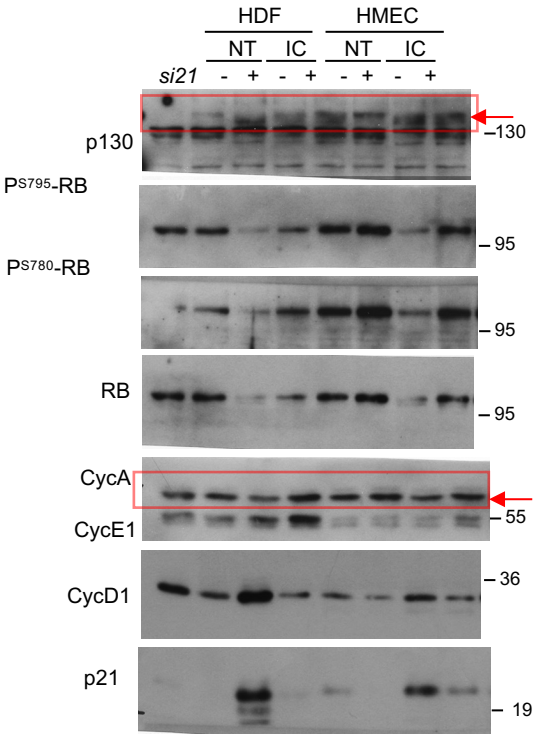

Figure 2H

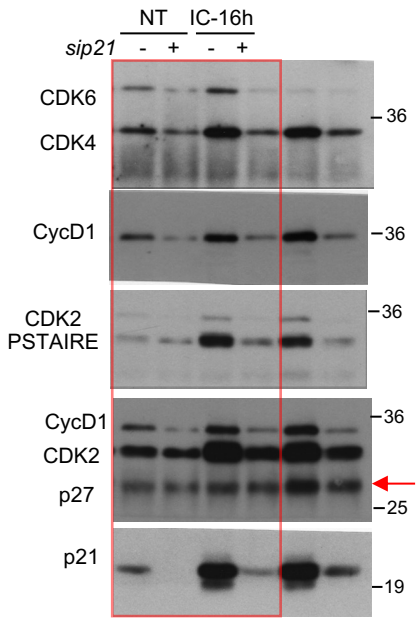

Figure 2I

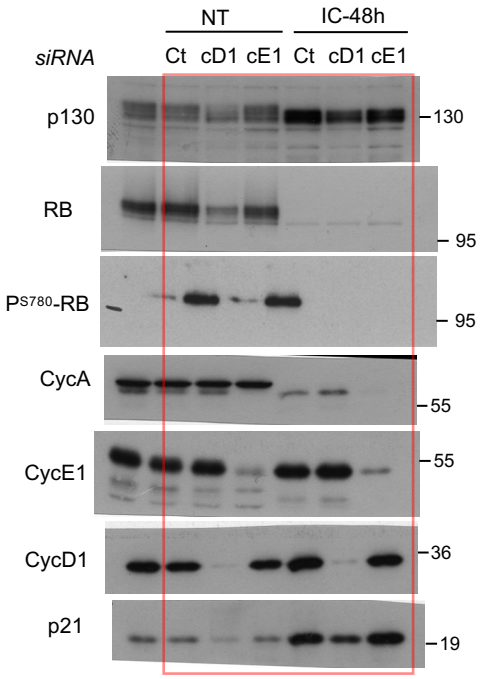

Figure 2SA

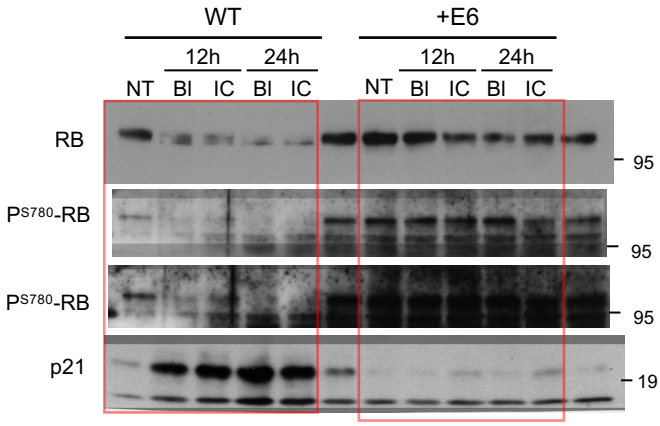

Figure 3A

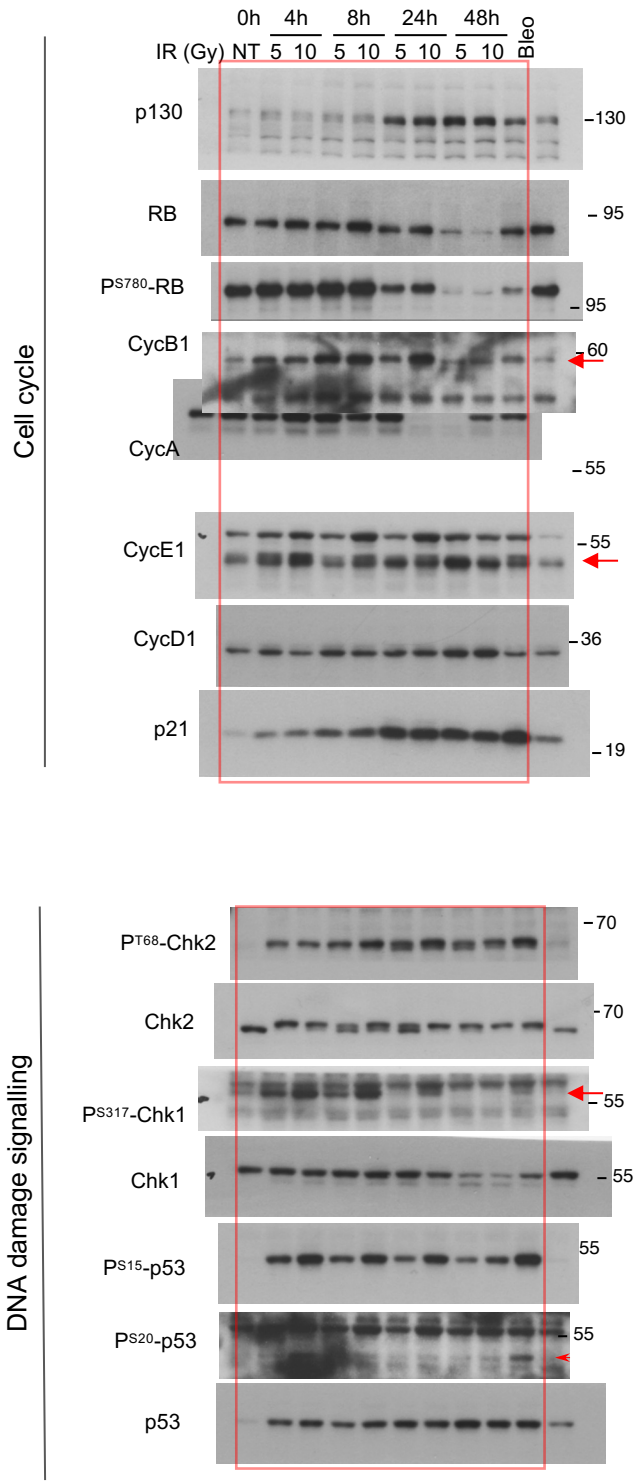

Figure 3D

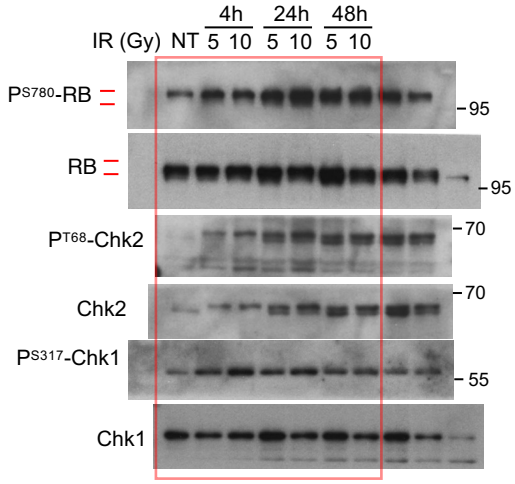

Figure 3F

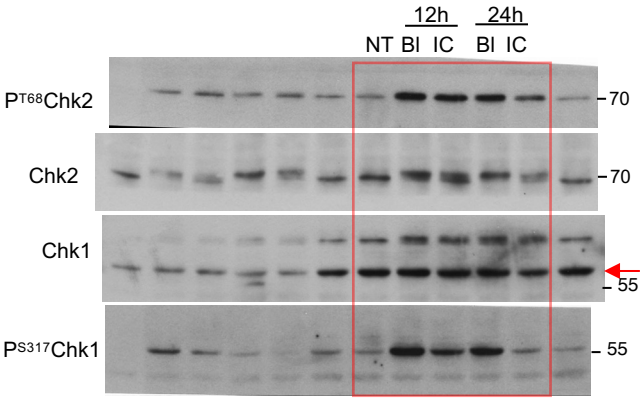

Figure S3C

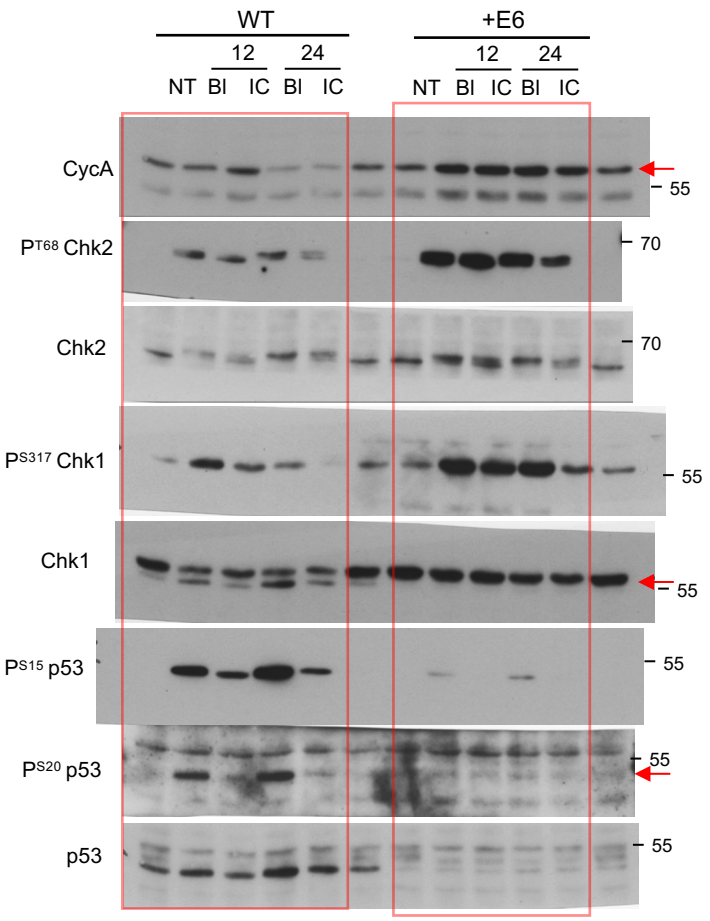

Figure S3D

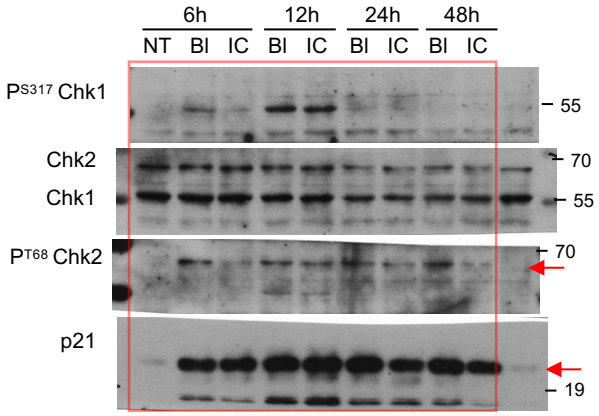

Figure S3E

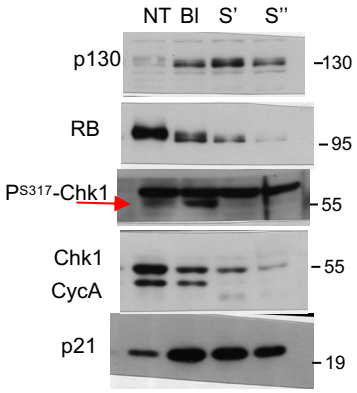

Figure S3F

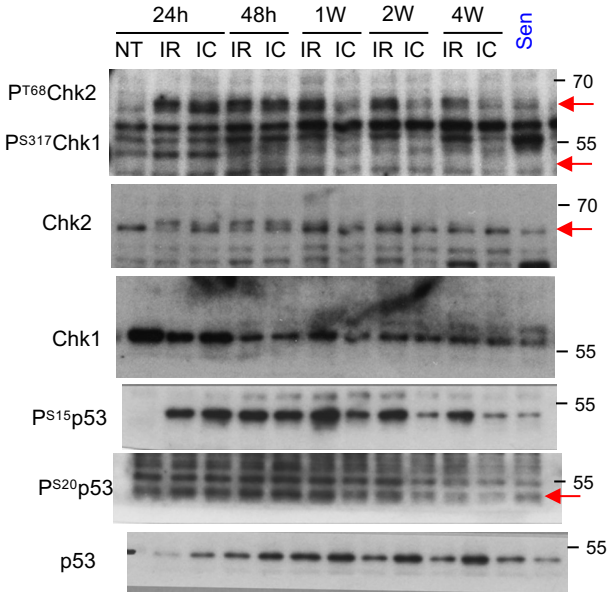

Figure 5B

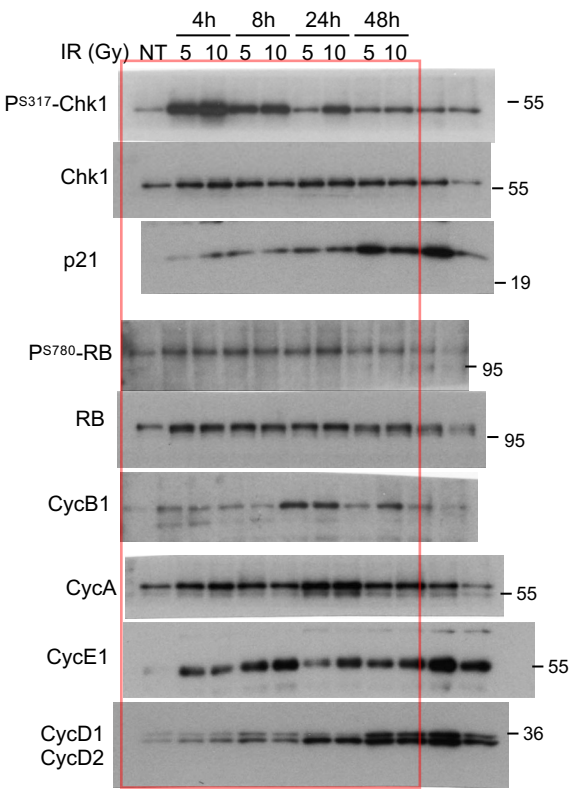

Figure 5H

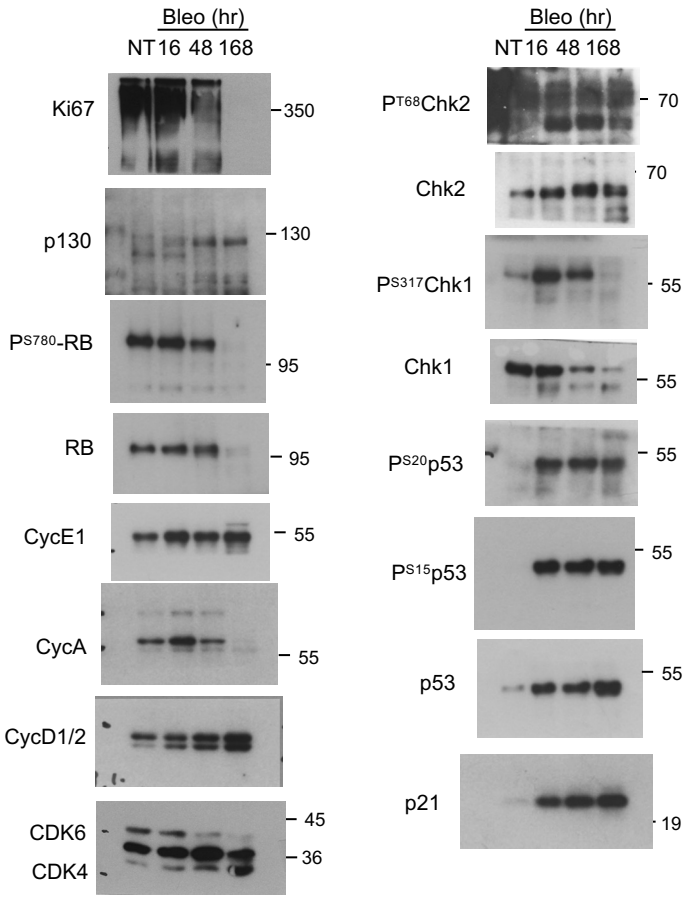

Figure S4B

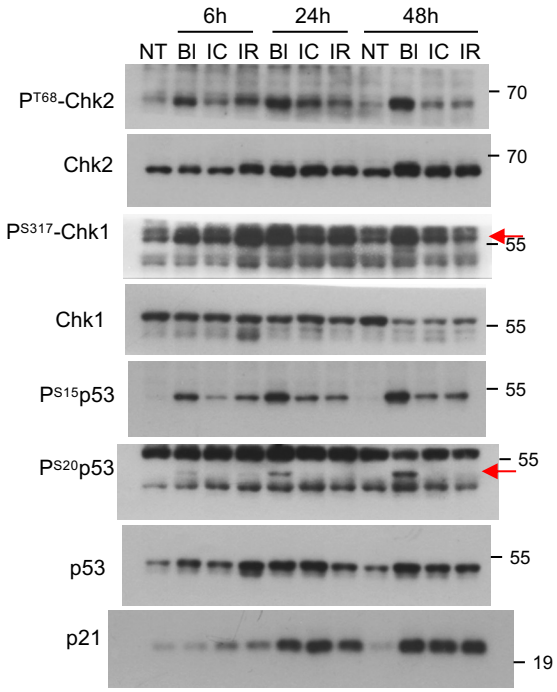

Figure S4C

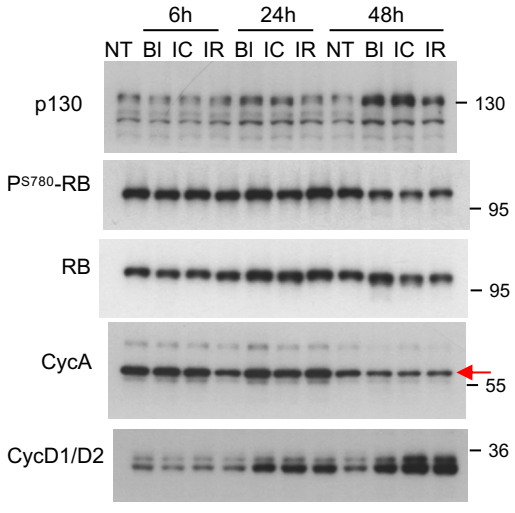

Figure 6D

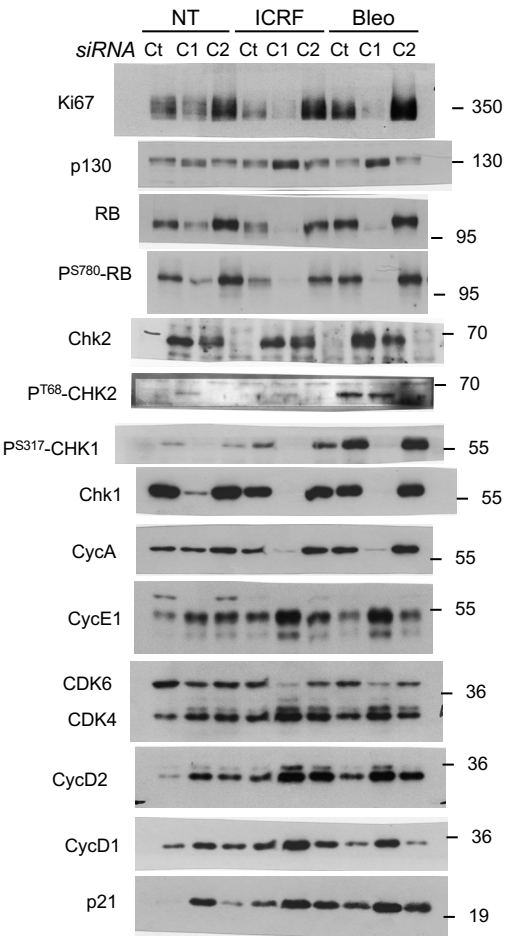

Figure 6E

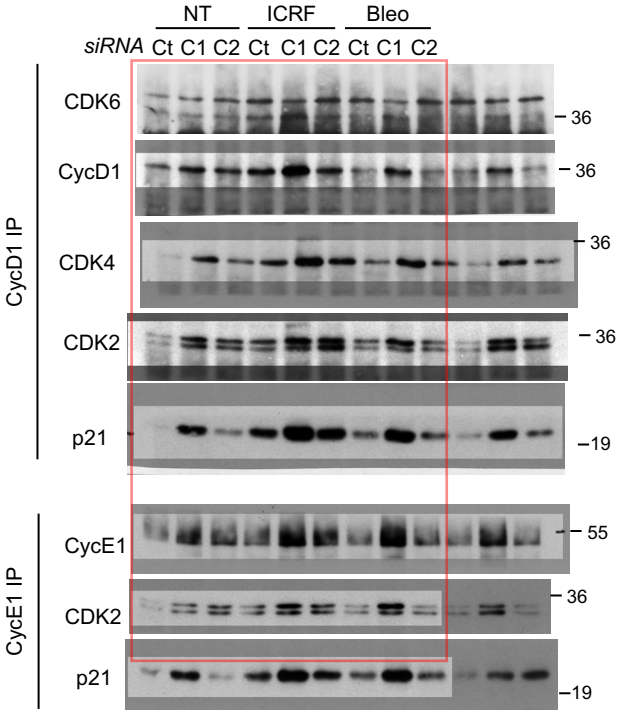

Figure 6F

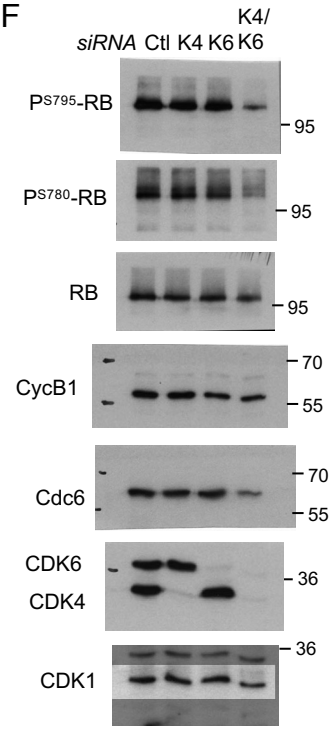

Figure S6B

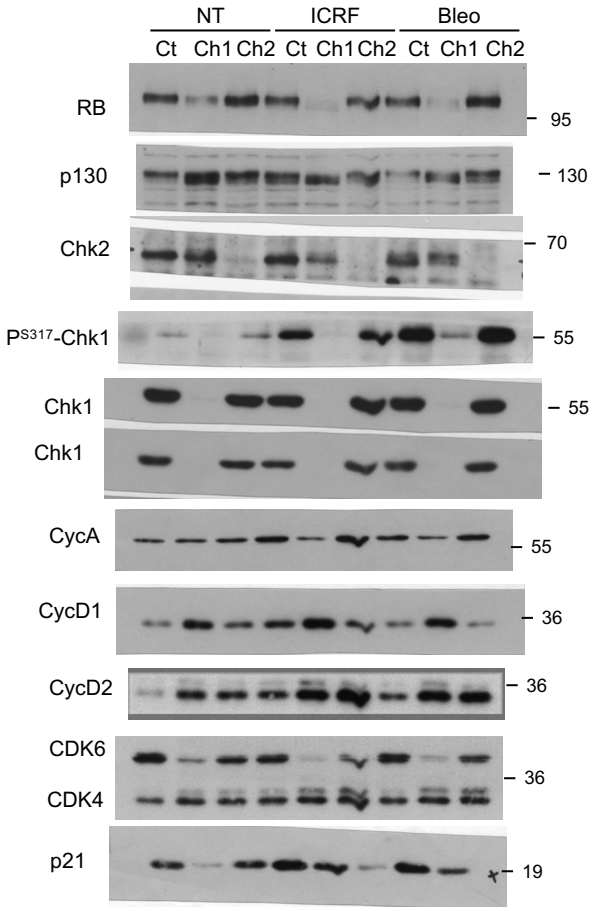

Figure S6C

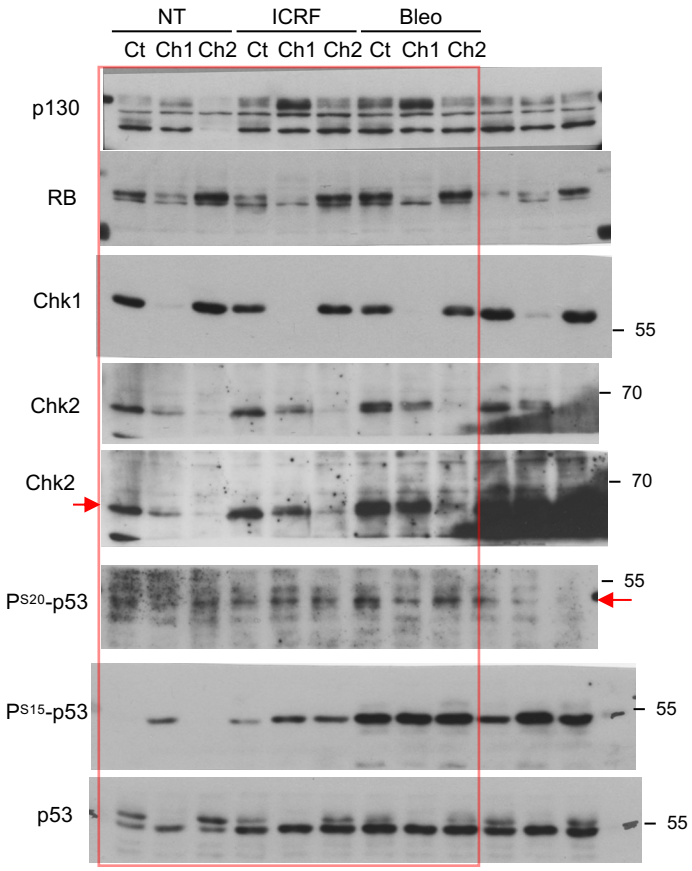

Figure S6E

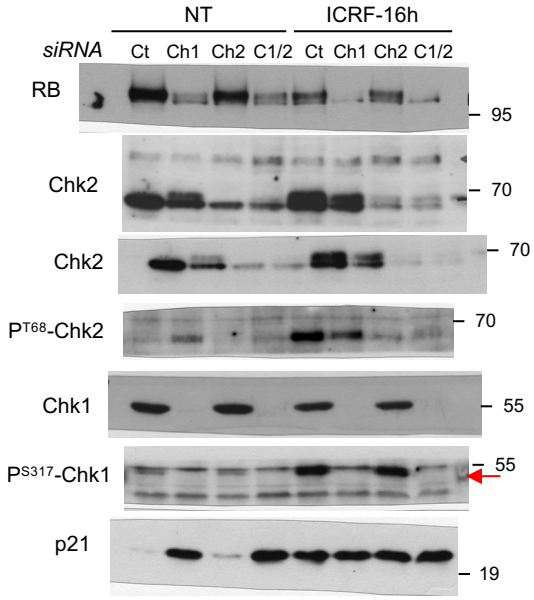

Figure 7B

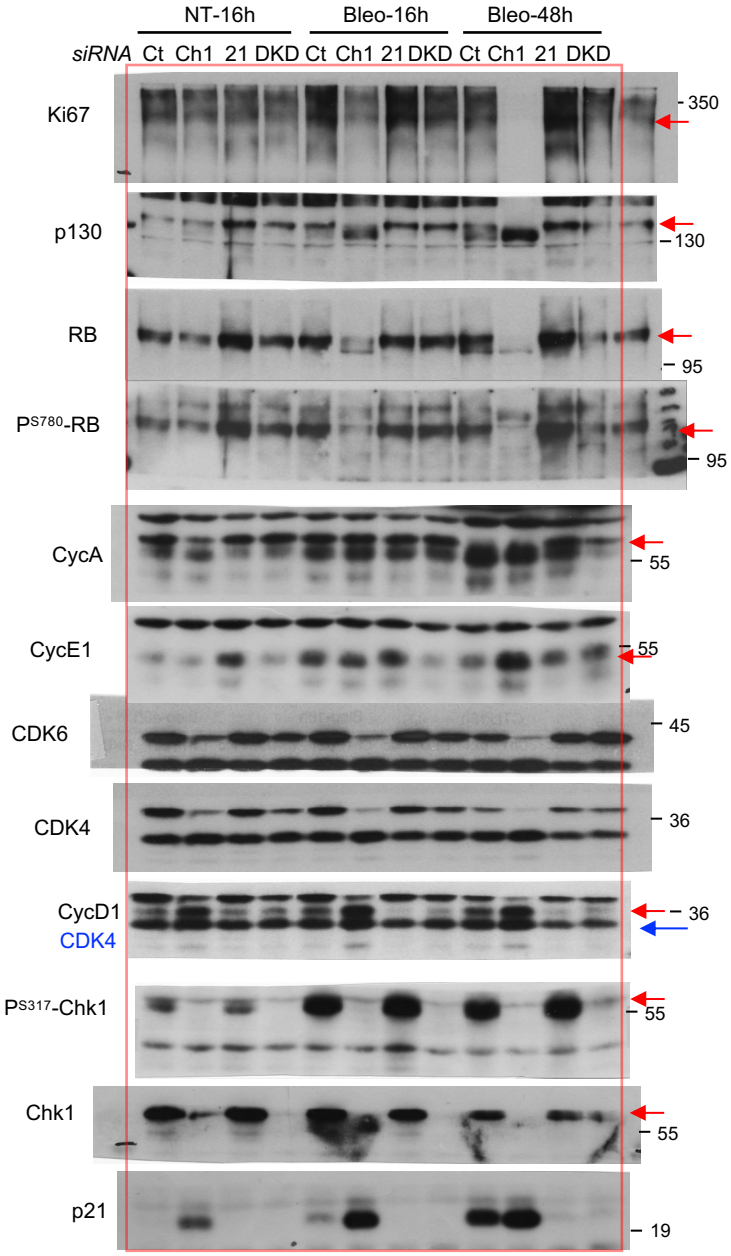

Figure 7C

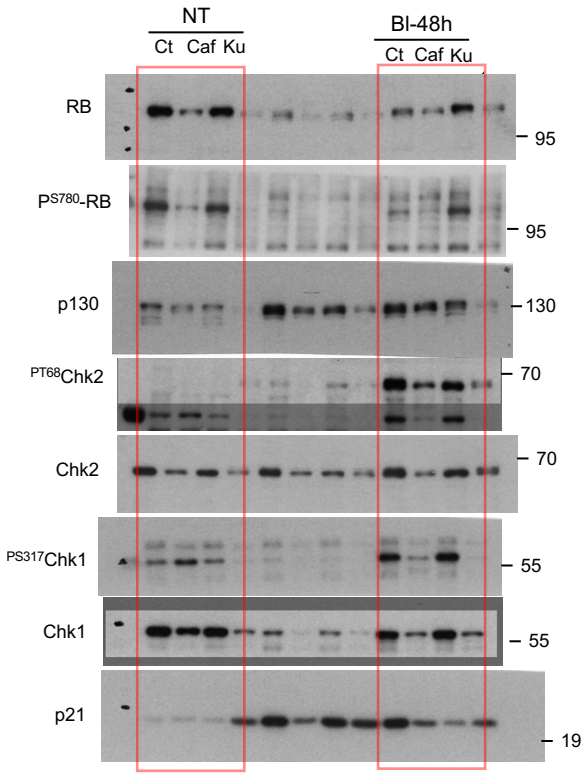

Figure 7F

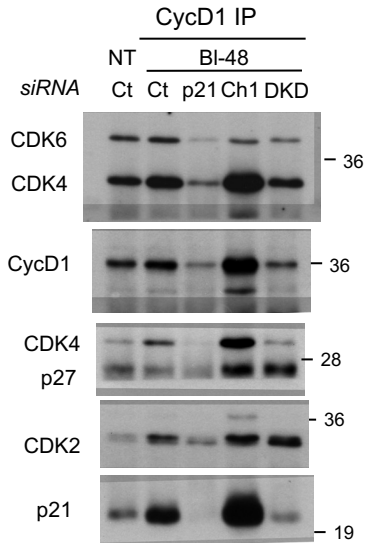

Figures 7E and S7F

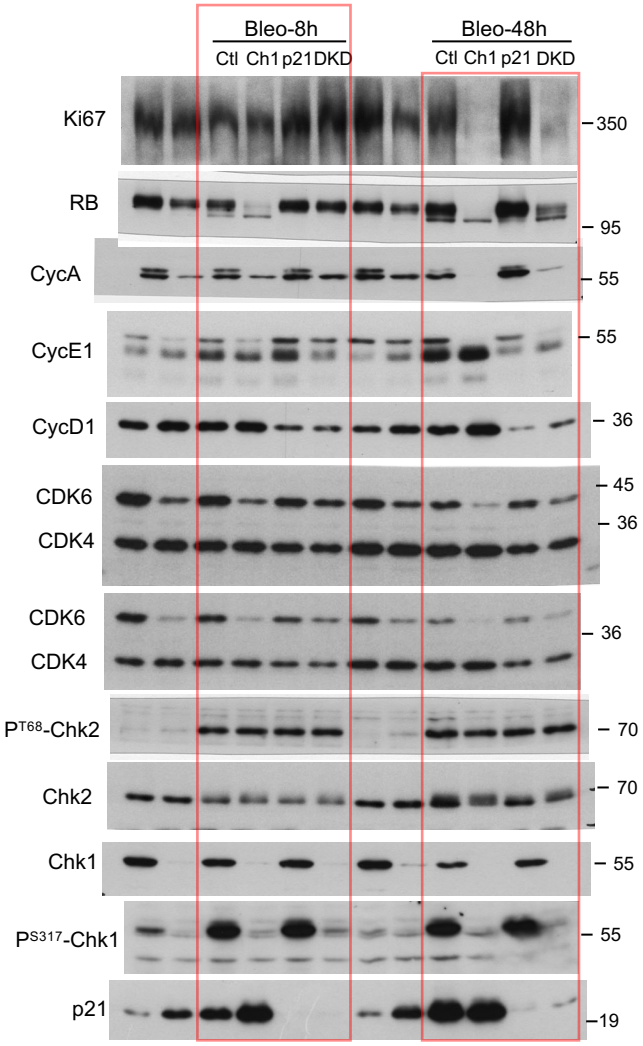

Figure S7B